The proposed Caroline ESA M3 mission to a Main Belt Comet

Available online at www.sciencedirect.com

ScienceDirect

Advances in Space Research 62 (2018) 1921–1946

ADVANCES IN SPACE RESEARCH (a COSPAR publication)

www.elsevier.com/locate/asr

The proposed Caroline ESA M3 mission to a Main Belt Comet

Geraint H. Jones [a,b,*], Jessica Agarwal [c], Neil Bowles [d], Mark Burchell [e], Andrew J. Coates [a,b], Alan Fitzsimmons [g], Amara Graps [h], Henry H. Hsieh [h,i], Carey M. Lisse [j], Stephen C. Lowry [e], Adam Masters [f], Colin Snodgrass [k], Cecilia Tubiana [c]

[a] *Mullard Space Science Laboratory, University College London, Holmbury St Mary, Dorking, Surrey RH5 6NT, UK*
[b] *The Centre for Planetary Sciences at UCL/Birkbeck, Gower Street, London WC1E 6BT, UK*
[c] *Max-Planck-Institut für Sonnensystemforschung, Justus-von-Liebig-Weg 3, 37077 Göttingen, Germany*
[d] *Atmospheric Physics, University of Oxford, Clarendon Laboratory, Parks Road, Oxford OX1 3PU, UK*
[e] *School of Physical Sciences, Ingram Building, University of Kent, Canterbury, Kent CT2 7NH, UK*
[f] *The Blackett Laboratory, Imperial College London, Prince Consort Road, London SW7 2AZ, UK*
[g] *Astrophysics Research Centre, School of Mathematics and Physics, Queen's University Belfast, Belfast BT7 1NN, UK*
[h] *Planetary Science Institute, 1700 East Fort Lowell Rd., Suite 106, Tucson, AZ 86719, USA*
[i] *Academia Sinica Institute of Astronomy and Astrophysics, P.O. Box 23-141, Taipei 10617, Taiwan*
[j] *Johns Hopkins University Applied Physics Laboratory, 11100 Johns Hopkins Road, Laurel, MD 20723, USA*
[k] *Planetary and Space Sciences, School of Physical Sciences, The Open University, Milton Keynes MK7 6AA, UK*

Received 30 April 2017; received in revised form 1 February 2018; accepted 25 February 2018
Available online 2 March 2018

Abstract

We describe *Caroline*, a mission proposal submitted to the European Space Agency in 2010 in response to the Cosmic Visions M3 call for medium-sized missions. *Caroline* would have travelled to a Main Belt Comet (MBC), characterizing the object during a flyby, and capturing dust from its tenuous coma for return to Earth. MBCs are suspected to be transition objects straddling the traditional boundary between volatile–poor rocky asteroids and volatile–rich comets. The weak cometary activity exhibited by these objects indicates the presence of water ice, and may represent the primary type of object that delivered water to the early Earth. The *Caroline* mission would have employed aerogel as a medium for the capture of dust grains, as successfully used by the NASA *Stardust* mission to Comet 81P/Wild 2. We describe the proposed mission design, primary elements of the spacecraft, and provide an overview of the science instruments and their measurement goals. *Caroline* was ultimately not selected by the European Space Agency during the M3 call; we briefly reflect on the pros and cons of the mission as proposed, and how current and future mission MBC mission proposals such as *Castalia* could best be approached.

Keywords: Asteroids; Comets; Interplanetary dust and gas

1. Introduction

Where does Earth's water come from? There are few questions about our planet's history that are more fundamental. Here, we describe a mission proposed to the European Space Agency that aimed to address this question, and many others, by visiting for the first time a member of a newly-discovered family of objects in our Solar

* Corresponding author at: Mullard Space Science Laboratory, University College London, Holmbury St Mary, Dorking, Surrey RH5 6NT, UK.
E-mail address: g.h.jones@ucl.ac.uk (G.H. Jones).

https://doi.org/10.1016/j.asr.2018.02.032
0273-1177/

System: Main Belt Comets (MBCs). These perplexing objects have stable orbits within the asteroid belt, but during certain seasons behave like comets, possessing a dust coma and tail. This strongly suggests that volatiles at their surfaces are sublimating, driving off the dust. This volatile material is likely to be water ice. Dynamical models suggest that bodies from this region brought water to Earth. The remaining MBCs are therefore believed to hold a frozen record of the source of Earth's water. The proposed mission's name—*Caroline*—was in honour of Caroline Lucretia Herschel (1750–1848), arguably the first great female astronomer, and discoverer or co-discoverer of at least six comets.

This highly focused small mission would have travelled to the MBC 133P/Elst-Pizarro to capture material from its dust coma/tail, bringing it back to Earth for highly detailed laboratory analysis. The capture of the dust would be achieved through the use of aerogel—an extremely low density material whose application to the collection of cosmic dust was very successfully demonstrated by NASA's *Stardust* mission to Comet 81P/Wild 2.

While capturing the dust from Elst-Pizarro, *Caroline* would scrutinize the nucleus with a visible camera and thermal infrared mapping spectrometer, searching for the source of the dust and mapping the body's surface morphology and mineralogy. A separate instrument would detect dust impacts on the spacecraft's protective shield.

MBCs are of particular interest to the planetary science community as they represent the "missing link" between rocky asteroids and icy comets. The population was only recognized in 2006, and has since been the subject of detailed scrutiny by planetary astronomers. They are dynamically stable now, but the may have formed beyond Jupiter and became trapped in the main belt in primordial times, when Jupiter was migrating (Walsh et al., 2011) or growing (Raymond and Izidoro, 2017), as indicated by cosmochemical studies (Kruijer et al., 2017). strongly implies that they formed where we observe them today. Their activity also suggests that volatile water-ice has been preserved in the subsurface layers since their formation. Most importantly, these objects are a likely source of water and therefore life on Earth. This presents a unique opportunity to probe pristine material from a known location in the protosolar disk. By imaging and sampling material via spacecraft fly-by, *Caroline* would have provided constraints on protoplanetary disk models, and would have helped answer key questions about how the Earth became the water-rich planet it is today and ultimately suitable for life. *Caroline* would have also contributed to an improved understanding of the formation and development of habitable planetary systems around our Sun and elsewhere.

As well as capturing Main Belt Comet dust and delivering it to us, *Caroline* would have also separately collected for the first time dust from the asteroid belt. This would likely have been a mix of material from numerous objects that would constitute a bonanza of new information in itself.

The mission would have launched on a Soyuz–Fregat rocket in late 2021, and following swing-bys of Venus and Earth, would fly past Elst-Pizarro in May 2025 with a low relative speed for dust capture. The capsule would have been returned to Earth in 2027. All the key technologies for this mission had been previously demonstrated, ensuring a robust, cost–effective spacecraft.

Addressing the ESA Cosmic Vision questions of "What are the conditions for life and planetary formation?" and "How does the Solar System work?", the proposers regarded *Caroline* as an excellent fit for addressing the agency's science goals. Building on the successes of previous small-body missions such as *Giotto*, *Stardust*, and *Deep Impact*, and following the then-anticipated wealth of results from *Rosetta* and *Dawn*, the proposing team believed at the time of proposal that *Caroline*, by visiting this newly-discovered class of objects, promised to provide a step-change in our knowledge of the early solar system, and in turn that of our own planet.

2. Scientific objectives and requirements

2.1. Introduction and mission overview

Asteroids and comets are of interest because they provide a way to probe the protoplanetary disk from which our solar system formed. By determining the chemical and physical properties of various populations of small bodies in our solar system, we can gain insight into the chemical and thermal conditions in different areas of the disk and also investigate the chemical, thermal, collisional, and dynamical processes that have shaped those populations since their formation.

Had the mission gone ahead, by returning a sample of ejected material from an active MBC *Caroline* would:

- Gather data critical for evaluating hypotheses concerning the primordial delivery of water and other volatile materials to Earth, shedding light on the question of how life itself came to be possible
- Explore a member of a newly discovered class of objects that challenges classical definitions of both asteroids and comets
- Bring the first-ever sample of material from the asteroid belt back to Earth, enabling detailed laboratory study of some of the most pristine material remaining in the modern solar system
- Greatly increase our understanding of the compositional and temperature structure of the protosolar disk, in turn providing insights into conditions that may give rise to habitable extrasolar planets

Previous missions to the main belt had visited inert asteroids but not MBCs, while cometary missions had visited Jupiter Family Comets and 1P/Halley. Sample return missions had at that time attempted to return material from near-Earth space, but no sample has been brought

back from the main asteroid belt from either an asteroid surface or an MBC. *Caroline* would be similar in some ways to the cometary mission *Stardust*, but would visit a completely different population of comets.

2.2. Background

Ice in Small Bodies The fraction and composition of ice in a body are of interest due to the temperature constraints that they provide and the importance of water to life on Earth. The "snow line" is the distance from the Sun at which water freezes into solid ice and can be incorporated into accreting planetesimals. The exact location of the snow line in our protoplanetary disk was dependent on various poorly constrained conditions including opacity, mass density, and accretion rate in the disk. As the disk evolved, the snow line is thought to have shifted as planetesimal accretion progressed (Oka et al., 2011). Bodies formed in the outer solar system between Jupiter and Neptune and beyond (the Kuiper Belt) are well beyond the snow line and thus are certainly icy. Closer to the Sun, the situation is less certain. Observations of asteroids suggest that the snow line probably existed around 2.5 AU from the Sun (Gradie and Tedesco, 1982; Jones et al., 1990), but theoretical studies (e.g., Sasselov and Lecar, 2000) have placed it possibly closer than the orbit of Mars. If true, objects throughout the main asteroid belt could have incorporated water ice at the time of their formation. However, Jupiter may have blocked the flux of icy particles towards the asteroid belt so that indigenous asteroids could not accrete much ice even if the disk became cold. In this latter scenario, water-rich asteroids would originate beyond the orbit of Jupiter. Cosmochemical studies provide support for such an interpretation (Kruijer et al., 2017).

Since their formation, asteroids in the main belt have undergone substantial heating from solar radiation, the radioactive decay of ^{26}Al, and perhaps electromagnetic induction from the solar wind that long ago caused that primordial water ice to liquefy and drive hydration reactions within the parent bodies (Grimm and McSween, 1989; Cohen and Coker, 2000; Mousis and Alibert, 2005). Spectroscopic evidence of these reactions exists in the form of absorption features in the infrared portion of the spectrum at 3 μm (e.g., Lebofsky, 1980; Lebofsky et al., 1981) and in the visible portion of the spectrum at 0.7 μm (e.g., Vilas et al., 1994; Barucci et al., 1998). Hydrated minerals have also been found in CI and CM carbonaceous chondrite meteorities that possibly originated from C-type or D-type asteroids in the main belt (e.g., Hiroi et al., 1996; Vernazza et al., 2013).

Given the ubiquity of primordial water implied by spectroscopic and meteoritic evidence, Jones et al. (1990) argued that a decline in hydrated silicate detections on asteroids with increasing semimajor axis could indicate not a lack of ice, but insufficient heating to melt that ice and drive hydration reactions. That ice could still exist today. By combining HST observations of the shape of asteroid 1 Ceres, the largest object in the asteroid belt, with other physical properties such as its rotation rate and bulk density, Thomas et al. (2005) demonstrated that Ceres is most likely a differentiated body consisting of a dense core of rocky material surrounded by a water-ice mantle comprising 16–26% of the total mass of Ceres. More recently, observations with the Herschel space telescope revealed outgassing of water (Küppers et al., 2014), and the Dawn mission confirmed the presence of (sub)-surface ice (Nathues et al., 2015; Combe et al., 2016; Platz et al., 2016).

Water ice has been detected spectroscopically on the surfaces of ~100 km diameter asteroids (Rivkin and Emery, 2010; Campins et al., 2010), although the interpretation of these results have been challenged (Beck et al., 2011). Centered at 3.1 μm, an absorption band unlike those caused by hydrated minerals in carbonaceous chondrites or C-type asteroids was observed in the near-IR spectrum of asteroid 24 Themis. Modelling of the absorption band indicated that it was likely due to fine-grained water ice and organic material. The absence of hydrated minerals on the surface of 24 Themis suggests that there could be a large continued presence of ice within the asteroid that could survive longer than the age of the Solar System (Campins et al., 2010). Exposure of this ice could be explained by impact events overturning the surface. A similar process occurs on the Moon at a rate of 1 m/Gyr. Alternatively, the slow sublimation of water ice could cause escaping water to recondense on the asteroid surface as a frost.

Studies on the survivability of ice in the main-asteroid belt suggest that water-ice can survive in subsurface layers. A general study by Schorghofer (2008) investigated the survivability of surface ice in spherical bodies at heliocentric distances of 2–3.2 AU. The models indicate that ice can persist in the top few metres of a dusty asteroid surface, if the surface temperature remains below 145 K. Although this favours ice retention on slowly rotating asteroids ice can still survive at high latitudes on fast rotating asteroids.

Main–Belt Comets Further evidence of present-day ice in main-belt asteroids came in 2006 with the discovery of the new cometary class of main-belt comets (Hsieh and Jewitt, 2006). MBCs occupy stable orbits in the main asteroid belt indistinguishable from those of other main-belt asteroids, yet exhibit cometary mass loss in the form of comae and dust tails, indicative of the sublimation of volatile ices. MBCs differ from other comets in that their stable orbits indicate they are most likely native to the inner solar system, having orbits that have been stable since the end of the era of giant planet formation/migration, whereas other comets originate in the colder and icier outer solar system in the Kuiper Belt or Oort Cloud.

Motivated by their study of comet 133P/Elst-Pizarro, the first known MBC (Hsieh et al., 2004), Hsieh and Jewitt set out to try to explain its strange comet-like physical behaviour but asteroidal dynamical properties by putting the two lead hypotheses for 133P's origin to the test. If

133P was a "lost comet", i.e., an ordinary comet from the outer solar system that had somehow dynamically evolved onto a main-belt orbit, it could be unique in the asteroid belt, given how difficult such a dynamical transition is considered to be. If, on the other hand, 133P was an icy asteroid that was native to the main asteroid belt, more 133P-like cometary asteroids would be expected to exist, since if 133P was an otherwise ordinary asteroid that happened to exhibit cometary activity, other otherwise ordinary asteroids could do so as well.

In 2005, whilst conducting a targeted survey of the outer main belt, Hsieh and Jewitt discovered another active comet, 176P/LINEAR. Together with the serendipitous discovery of another comet in the asteroid belt, 238P/Read, 133P and 176P constituted a new class of cometary objects, dubbed MBCs (Hsieh and Jewitt, 2006; Hsieh et al., 2009). The small scale of their survey (just 600 objects observed, out of more than 400,000 main-belt objects known at the time) further suggested that the total size of the active MBC population could be much larger, possibly in the hundreds (Hsieh et al., 2009). While fulfilling a key prediction of the "icy asteroid" hypothesis (that 133P would not be unique), the discovery of multiple objects in the asteroid belt exhibiting cometary behaviour rendered the "lost comet" hypothesis extremely unlikely, given the vanishingly low likelihood of multiple outer-solar-system comets transitioning onto main belt orbits.

More MBCs have been found since 2006, validating the prediction that the first three MBCs represent a small sample of a larger population. There are now five known MBCs with confirmed repeating activity in multiple orbits, and a total of 18 "active asteroids", including objects which may be genuine MBCs and others that have the appearance of comets due to dust release in collisions, for example. With the advent of modern sky surveys like Pan-STARRS, the discovery rate is now approximately 1/year (Hsieh et al., 2015), although confirmation of ice-driven activity normally requires observations in at least two orbits, meaning a 5–6 year wait. Modelling of coma morphology that indicates long-lasting release of dust rather than an impulsive event can give a strong indication that a candidate is likely to be a true MBC. Candidates discovered within the same dynamical family as previous MBCs, e.g. the Themis family, are also more promising. A table of all current MBCs and candidates can be found in the paper describing the *Castalia* mission elsewhere in this issue (Snodgrass et al., 2018). Reviews of recent results, including discussion of the various dust release mechanisms relevant for asteroids and the challenges associated with directly identifying water in MBCs, are included in Snodgrass et al. (2017).

The Mystery of Earth's Water One of the major areas of interest in planetary science and astrobiology concerns the origin of water and other volatile material on the Earth. Given our current understanding of the solar system's formation, the Earth likely formed well inside the snow line, and as a result, should not have accreted a significant amount of water ice and should be largely dry (e.g., Boss, 1998). Drake (2005) suggest that "wet accretion" could also be possible, but the more generally-held view of "dry accretion" is corroborated by the distribution of asteroids in the main belt, where evidence of hydration is only seen on asteroids outside of 2.5 AU from the Sun (Gradie and Tedesco, 1982), well beyond Earth's orbit. The dry character of the Earth, S-type and E-type asteroids can also be explained if Jupiter intercepted the flux of icy particles towards the inner solar system (Morbidelli et al., 2016; Kruijer et al., 2017). Whatever scenario led to the Earth accreting from mostly anhydrous planetesimals, as it appears to have done so, it should therefore be anhydrous itself. Since the present-day Earth is not dry, we are left to determine the source of our current water.

There are three primary scenarios for the origin of water on Earth:

1. *Endogenic*: In this case, the water was not brought to Earth; it was already here, due to various suggested scenarios (Ikoma and Genda, 2006; Stimpfl et al., 2006; Genda and Ikoma, 2008; Muralidharan et al., 2008). In the first case, 13 Earth oceans of water could be adsorbed by associative adsorption onto perfect forsterite surfaces, while later studies of imperfect forsterite suggest more Earth oceans of water were adsorbed prior to planetary accretion onto the building blocks of terrestrial planets (Muralidharan et al., 2008).In the nebular origin model, Earth attracted the surrounding nebula gas to have a massive ($>10^{21}$ kg) hydrogen-rich atmosphere. At the time, our planet was covered in a magma ocean containing oxides such as FeO that reacted with the hydrogen to produce water. The surrounding nebular gas then began to disappear, the dense atmosphere and proto-Earth cooled, and 1–100 ocean masses formed through the condensation of steam in the atmosphere (Genda and Ikoma, 2008). When the nebular gas dissipated enough to permit the extreme- ultraviolet and far-UV radiation from the Sun to penetrate the Earth's atmosphere, the lightest gases, hydrogen and helium, escaped into space.
2. *Exogenic* ("stochastic, big splashes model") (O'Brien et al., 2006; Raymond et al., 2004; Morbidelli et al., 2000; Raymond and Izidoro, 2017; O'Brien et al., 2014): The water came from agglomerated bodies on solar orbits inside of Jupiter's orbit. These chance occurrences, primarily after Earth had formed but before the Moon-forming impact, brought the water and volatiles to Earth. This terrestrial planet formation scenario works best after 10 My, by which point the nebular gas has dissipated. The amount of water accreted by their modelled terrestrial planets.
3. *Both Endogenic and Exogenic* (a "dual-origin model"): The proto-Earth picked up water from nebular gas or planetesimals, but then the lighter gases escaped hydrodynamically. After the nebular gas dissipated, but before Earth's last major impact (the moon-forming event), a

few impacts of (cold) comets travelling from the outer solar system supplemented the Earth's noble gas inventory.

Estimates for the contribution to Earth's oceans from Oort cloud comets range from less than 10% (Robert et al., 2000) to 50%. Theoretical arguments rule them out as the only source of Earth's water because many more comets would exist in the outer parts of the solar system than is currently thought to be possible (Morbidelli et al., 2000). So then, if not Oort Cloud comets, what brought the water to the Earth? A possibility are Jupiter-family comets, but as discussed above, certain main-belt asteroids could also contain substantial amounts of ice and therefore should also be considered.

Isotopic Constraints The deuterium to hydrogen (D/H) isotopic ratio is commonly used to trace the formation location of water ice: Substitution of one hydrogen atom in water results in deuterated water, HDO, and proceeds by the reversible reaction

$$H_2O + HD = HDO + H_2 \quad (1)$$

In the early solar nebula, this reaction occurred while water was still in the vapour phase, leading to a reduction in HDO. After condensation and formation of ice grains, the reaction halts. Therefore, the reaction slows and halts more rapidly at larger heliocentric distances. This leads to an enrichment of the D/H ratio at larger heliocentric distances (Robert et al., 2000; Mousis et al., 2000; Horner et al., 2007). The ice grains continue to grow and are incorporated into the planetesimals of the early Solar System, with the D/H ratio tracing the ice formation region.

Earth's oceans have enhanced D/H relative to the solar nebula value. D/H in Standard Mean Ocean Water (SMOW) is 1.6×10^{-4} (Balsiger et al., 1995). This is 6–7 times the values deduced for the primitive Sun (Robert et al., 2000; Robert, 2001). Measurements of D/H in Oort cloud comets generally have a significantly higher value than SMOW (Balsiger et al., 1995; Eberhardt et al., 1995; Meier et al., 1998; Bockelée-Morvan et al., 1998; Weaver et al., 2008; Villanueva et al., 2009). Dust returned by the *Stardust* mission to Comet 81P/Wild 2 revealed a wide range of values between SMOW and a few times this (McKeegan et al., 2006). Results obtained after *Caroline* was proposed first indicated that Jupiter family comets (from the Kuiper Belt) were a good match to Earth's water, based on *Herschel* space telescope observations, and then conclusively demonstrated that they cannot be the main source, when *Rosetta* showed comet 67P/Churyumov-Gerasimenko to have a value $\sim$ 4 times SMOW (Hartogh et al., 2011; Lis et al., 2013; Altwegg et al., 2015).

Coupled with the inferred and observed existence of ice in the main asteroid belt, the MBCs present themselves as excellent candidates to probe the nature of water ice in the main asteroid belt and thus to test the exogenic origin of Earth's water. By measuring the D/H ratio we would be able to validate or dismiss this hypothesis. Although telescope observations are being used increasingly to measure the D/H ratio, it is only possible when the targets are exceptionally bright. Measurement of this ratio for MBCs via telescopic observations is impossible due to their faintness, and will remain so even with the next generation of space- and extremely large ground-based telescopes (Snodgrass et al., 2017).

Since the impact of comets would have raised the D/H ratio on Earth, it could be expected that D/H measured in the MBCs would be lower than SMOW. Coupled with noble gas measurements from the returned sample, we would be able to determine the likelihood that the MBCs are the sources of Earth's water. We could also be able to constrain the cometary contribution further, complementing results based on *Rosetta* data (Marty et al., 2016, 2017). In each case, when combined with data from the sample return and in-situ study performed by *Caroline*, we would be provided with information to help constrain where in the Solar System the MBCs formed relative to comets, S- and C-type asteroids. This knowledge would aid our understanding of the dynamical evolution of the Solar System, the chemical and thermal properties of the protoplanetary disk, and most importantly, could help determine the likely delivery method of water to Earth.

3. Scientific strategy

The strategy for deriving the maximum scientific return from the *Caroline* mission consisted of three components: remote observing, *in situ* analysis, and sample return.

The *Caroline* primary target, 133P, was already fairly well-characterized at the time of the proposal (Hsieh et al., 2004, 2010) following 15 years of Earth-based observations. Its active seasons are well constrained, and have been used to model the activity as due to a single active patch at mid latitudes on the surface. Its approximate shape is known from light-curves, and its albedo has been estimated (Hsieh et al., 2004, 2009). The properties of its surface material have also been probed using polarimetry (Bagnulo et al., 2010). Additionally, there are ongoing observation campaigns to further improve our knowledge of the properties of MBCs, including surveys to find more of these objects and follow up studies on all known ones. In the case of 133P, further ground based observations would allow the determination of a more complex shape model and pole solution using the light-curve inversion method (Kaasalainen and Torppa, 2001), refinement of the rotation period, and more precise measurements of the exact dates of active periods. Together these would allow more detailed modelling of the size and location of the active area(s) ahead of *in situ* observation by the spacecraft. These studies would also give similar details on other MBCs, which would potentially produce other suitable alternative targets for the mission.

In addition to the information found by analysis of returned coma and tail dust, a great deal of information

could have been obtained by remote sensing instruments. The most important such instrument would have been a visible imaging camera system (VCS), which would measure the basic bulk properties of the nucleus (size, shape, surface albedo), would allow studies of surface morphological features (craters, active areas), and also be used to map jets and other coma features. The proposed camera was based on the flight proven design for the Dawn Framing Camera (Sierks et al., 2011). In addition to science, the optical camera would be used for navigation.

Six comets have been visited by spacecraft with operating cameras (Jones et al., 2017). These are 1P/Halley (*VeGa–1*, *VeGa–2*, and *Giotto*; Keller et al., 1986), 9P/Tempel (*Deep Impact*; A'Hearn et al., 2005 and *Stardust-Next*, e.g. Li et al., 2013), 19P/Borrelly (*Deep Space 1*; Soderblom et al., 2002), 81P/Wild (*Stardust*; Brownlee et al., 2006), 103P/Hartley 2 (*EPOXI*; A'Hearn et al., 2011), and 67P/Churyumov-Gerasimenko (*Rosetta*; Sierks et al., 2015).

These missions revolutionized our knowledge of comets. The Halley encounter provided the first ever image of a comet nucleus, confirming Whipple's nucleus and coma model of comets. The images returned by subsequent missions revealed nuclei to be a diverse collection of objects with irregular shapes and varying morphology. They have some common features, such as very dark surfaces and activity from discrete areas of the surface, but also demonstrate a range of surface features from large smooth areas associated with activity (9P, 103P) to circular crater-like features (81P). The flyby of 103P showed an elongated nucleus with both rough terrain at the ends and a smooth waist. Images with narrow-band filters showed that the majority of the activity came from jets of CO_2 punching through the rough terrain, while lower level water driven activity was associated with the smooth waist. In the past few years the *Rosetta* mission has studied 67P in exquisite detail: Mapping surface features and following their evolution, sampling the dust and gas coma to measure composition at an isotopic level, and performing the first (and second) soft landing on a comet. Highlights of the results to date from this vast data set are reviewed by Taylor et al. (2017).

In contrast to comets, asteroids have old surfaces whose evolution is driven by impacts rather than erosion by activity. Spacecraft have taken images of several asteroids (including one binary system), mostly as fly–bys *en route* to other targets. The images returned by these missions varied in resolution due to the different instruments and flyby distances, but all revealed heavily cratered terrains and in many cases the existence of very large craters (relative to the size of the asteroid). There is some diversity in surface features, which appears to be most strongly controlled by the size of the asteroids. The tiny Itokawa was shown to be a "rubble pile" made up of loose rock (Fujiwara et al., 2006), while the 100 km scale Lutetia appears to be a solid body that has been at least partially shattered by impacts (Sierks et al., 2011). On Lutetia there are clearly terrains of different ages; old terrain is saturated with craters while younger terrain is covered in ejecta from a large recent crater (Thomas et al., 2012). Other geological features seen on asteroids include landslides, boulders, cracks, and grooves.

Nucleus morphology The primary goal of the imaging system would have been to reveal morphological features on the surface of the nucleus during the fly by. This would immediately answer one of the key questions about MBCs: compared to previous spacecraft images of comets and asteroids, do they appear comet-like or asteroid-like? Crater counting (e.g. Burchell and Kearsley, 2009) can reveal the ages of the surface, including identifying regions of different relative ages. If MBC activity alters the whole surface, then few craters would be seen, but we expect MBCs to have localized active regions, and as such, expected to have seen areas with young surfaces and also older "asteroidal" terrain away from the active regions. Any large craters would have allowed us to probe the internal structure of the MBCs, giving clues on the strength and composition of the interior.

The most important feature that would be observed on the surface of an MBC nucleus would be the active area. The source of activity is expected to be a relatively small patch of excavated ice, with an area of $\sim$100 m^2 (if pure ice; larger if the ice is covered with dust). Imaging of the nucleus would have provided a direct test of this hypothesis, as this area would be identifiable through either distinct morphology (smooth active-comet-like terrain, and/or a fresh crater); distinct reflectance properties (brighter and/or different colour) indicating a "fresh" surface, or visible links with jets of material imaged in the coma. On other comets there are multiple active areas and many coma jets; the behaviour of the MBC was expected to be simpler, with a single source of activity.

Shape and density Images of the nucleus would also reveal its bulk size and shape. Comets and asteroids have been found to be irregularly shaped bodies, and ground based observations of Elst-Pizarro suggests that it is an elongated body with dimensions of approximately $4.6 \times 3.2 \times 3.2$ km (for an assumed ellipsoidal shape). The true shape would of course be much more complicated, and a detailed model of this from spacecraft observations would give a precise measurement of the nucleus's volume. This would have then allowed us to measure the bulk density by combining this with the measurement of the mass of the nucleus obtained by radio science investigation during the fly by (Doppler shift in the signals from the spacecraft due to acceleration in the gravitational field of the MBC). The density is critical to understanding the interior of the nucleus; a low value (0.6 gcm^{-3} is a typical value for comets) would imply a large fraction of ice within the body and/or high porosity, while values more typical of asteroids (2–3 gcm^{-3}) would imply that MBCs are primarily rocky bodies with a small fraction of ice. As the mission's primary aim would be searching for the source of Earth's water, this measurement of the ice content of an MBC is a critical parameter.

Reflectance properties A direct measurement of the geometric albedo tells us about the surface composition; comets are exceptionally dark compared with asteroids and all other solar system bodies, which is thought to be due to a coating of organic material. Furthermore, we would have searched for variations in albedo that would show alteration to the surface, for example due to activity uncovering previously buried material, or coating the surface with particles from deeper within the nucleus. MBCs are expected to have only small active areas on otherwise inert bodies, so the differences in the surface between the active (comet like) and inactive (asteroid like) areas would be of great importance in understanding the process of cometary activity. There are likely to be differences in the spectra of different areas. These would be revealed by multi-colour imaging, with filter bandpasses selected to cover the full sensitivity range of the CCD from UV to near-IR.

Coma structures A critical goal of the VCS would be the mapping of structures within the coma. This would have been performed in the approach phase and also in detail around the closest approach. As the activity of MBCs is expected to come from a single active area, we expected a single jet (or possibly broad fan) of dust from a single site. The weak activity and distance of MBCs makes this impossible to do from Earth. The EPOXI mission was able to link jets directly to active areas on the nucleus of a comet, and also found highly active jets driven by CO_2 and weaker activity driven by water ice sublimation. For this reason, the VCS would include narrow band filters covering the emission wavelengths of these species to identify the gas responsible for the MBC activity. Identifying the jets of material would also be important for sample collection: the *Stardust* team was able to link the 3D structure of jets seen in the coma to clusters of particle impacts on their dust detectors.

Required resolution and coverage As a key goal of our imager was to resolve active areas of tens of metres in diameter, we required metre-scale resolution. The use of the Dawn Framing Camera design would have achieved this with a flight proven instrument. At close approach (50 km) when dust collection would occur, the long axis of 133P (4.6 km) would nearly fill the field of view of the camera ($5.5 \times 5.5^{\circ}$), giving a surface resolution of $\sim$5 m/pixel. This is comparable to the EPOXI mission to 103P/Hartley 2, and would have allowed the comparison of features of similar size.

At a flyby speed of 4.5 km s^{-1}, the nucleus would first be resolvable (2 pixel diameter) $\sim$1.5 h before closest approach, CA, and would present images useful for studying topography (diameter >10 pixels) 20 min before CA. Decametre-scale resolution would be possible for about two minutes around CA. The rotation period of 133P is 3.5 h, meaning that the majority of the surface would have been illuminated and visible to the spacecraft at some point while the nucleus was resolved. Constraints on the rotation pole were not strong at the time that the proposal was written; they would have been improved by further observations in the subsequent few years. However, extreme obliquities had already been ruled out: there was no expectation of a large "permanent winter" area that would remain dark during the flyby. This means that we would have been able to obtain an accurate shape model for the nucleus.

The CA time would have been adjusted to ensure the active area was visible to the spacecraft during this period. The position of the active area on the nucleus is already constrained by ground based observations (Hsieh et al., 2010). Further ground based observation leading up to the encounter and imaging of the coma and jets by the spacecraft on approach would have allowed further refinements in the weeks before the CA.

Mid-infrared spectroscopy A mid-infrared imaging spectrometer would serve two key purposes in characterising the geological context and structure of the object encountered by the *Caroline* spacecraft.

1. Production of compositional maps of the surface mineralogy of the object complementing VCS reflectance measurements
2. Determination of the physical nature and structure of the near-surface layers using thermophysical maps of the object's surface

Temperature mapping By providing accurate maps of surface temperature at tens of metres resolution, the instrument would have allowed the relationship between localised changes in albedo, surface temperature and volatile trapping and release to be studied. Localised regions of active volatile release would have been easily and quickly located due to their temperature depression. We would have been particularly interested in how regions on the surface become "activated", and how deposition of fresh material changes albedos and equilibrium temperatures. Measurements of the Moon (e.g., Paige et al., 2010, Fig. 1) and Iapetus (Spencer and Denk, 2010) have shown that the radiometric surface temperature can give important information on the trapping and migration of surface volatiles, and this would be especially important for understanding how MBC activity evolves with time.

Surface composition A mid-infrared (IR) thermal imaging spectrometer would have provided compositional maps of the surface mineralogy of the target object, complementing any near-IR reflectance spectroscopy measurements and providing the only remote sensing compositional information in any regions of shadow or night. The mid-IR is particularly well suited to distinguish silicate mineralogy that is inaccessible in the near-IR. This has been shown by the TES and THEMIS instruments on NASA's Mars Global Surveyor and Mars Odyssey spacecraft (e.g. Christensen et al., 2004) and on airless bodies by the Lunar Diviner Radiometer experiment on NASA's Lunar Reconnaissance orbiter (e.g. Greenhagen et al., 2010).

Disk averaged measurements of, e.g., the Trojan asteroids by the Spitzer space telescope have shown diagnostic

absorption features (Emery et al., 2006), and so can provide information on composition. Spatially resolved thermal infrared spectra are especially powerful when combined with near-infrared spectroscopy, where the data sets from the two instruments can be used to break compositional degeneracies (Donaldson Hanna et al., 2014).

The range of minerals (e.g. Fig. 1), volatiles and possibly organics present on objects such as 133P would make it a rich compositional target in the mid-IR and provide vital information on the chemical reprocessing that may have occurred on or near its surface.

Surface thermophysical properties Low (R<20) resolution thermal spectroscopy can also provide information on the temperature variation across 133P. This dataset is of great importance for mapping potential volatile reservoirs, changes in surface texture due to outgassing and also any changes in orbit/spin.

By accurately mapping the thermal emission from the object, the nature and structure of the surface and near subsurface could have been determined. In particular, by measuring the infrared thermal emission continuum from, e.g., 5 to 25 μm (a wavelength range not covered by *Rosetta*), the total flux, color temperature, and thermal inertia could be found, providing essential information on the small-scale structure of the surface via its day/night heating and cooling rates. The thermal inertia is defined as $\sqrt{k\rho c}$ with k the thermal conductivity, ρ the density and c the heat capacity of the surface, giving important information on the packing of surface material and bulk composition. Fig. 2 shows the expected diurnal surface temperature ranges anticipated for an object at an orbital distance of 2.641 AU (perihelion distance of 133P), a Bond albedo of ~0.05, and rotation period of 3.5 h for two different thermal inertias (to simulate changes in surface structure and composition) The solid line shows the case for a typical powder-like regolith, similar to that found on the Moon (Spencer et al., 1989); the dashed line for a shallow regolith/water ice mixture (Bandfield, 2007) such as may be present near the polar sub- surface of Mars. The model profiles are highly variant, and easily distinguished by current Fourier Transform Spectroscopy capabilities. Distinguishing the composition of the near-subsurface would

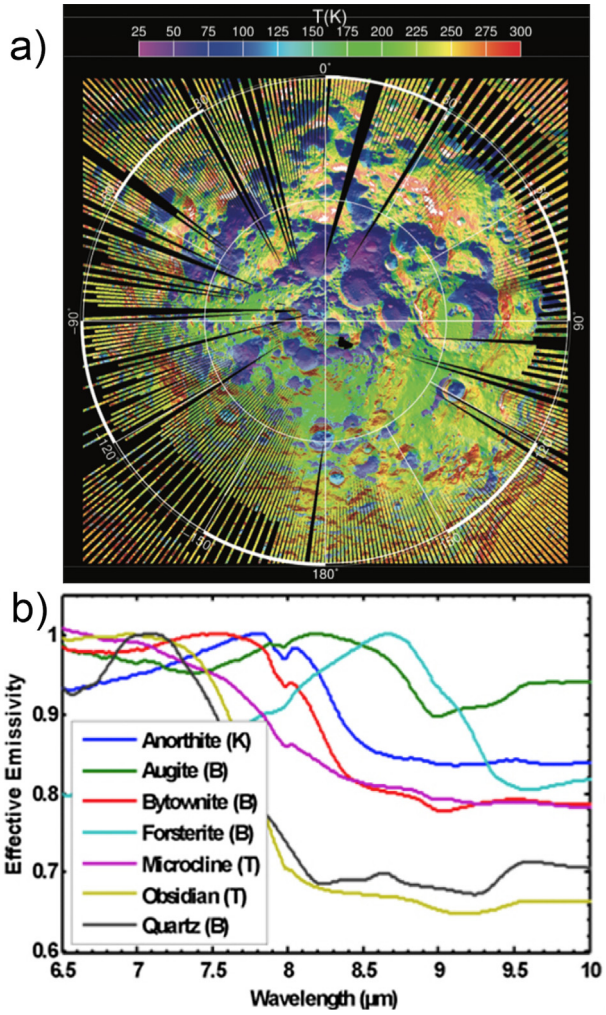

Fig. 1. (a) Cold traps at the Lunar South Pole measured by the Lunar Diviner Radiometer Experiment (adapted from Paige et al., 2010) (b) Example laboratory thermal emission spectra (Thomas et al., 2010) measured under a simulated space environment. The emission maximum located near 8 μm (the Christiansen feature) is particularly diagnostic of silicate mineralogy.

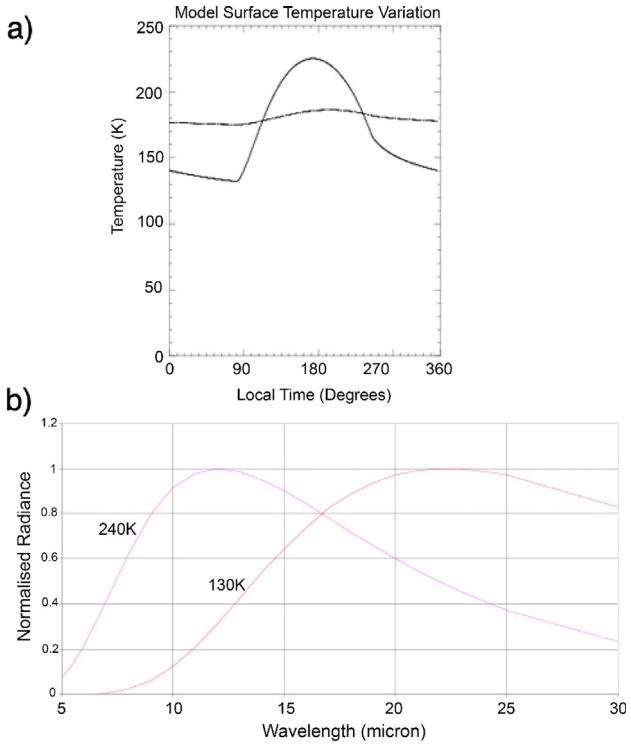

Fig. 2. (a) Diurnal temperature variation for an object with thermal inertial 50 J m^{-2} s^{-1}/2 K^{-1} and 800 J m^{-2} s^{-1}/2 K^{-1} using the thermal model described in Spencer et al. (1989), for an object at 2.641 AU, 3.5 h rotation period and a surface Bond albedo of 0.05. (b) Normalised Planck functions showing required wavelength coverage for the thermal infrared instrument.

have been vital in understanding how regions act as reservoirs for volatiles and how they become active or dormant. Given this expected diurnal temperature range of ~130–240 K, a thermal infrared instrument with a spectral range from 5 to 25 μm was deemed necessary to accurately determine the surface temperature variation. Based on our simple model, a scene temperature accuracy of ±3 K was have been needed to return useful thermal maps of the *Caroline* target.

A mid-infrared thermal–IR instrument, through determination of surface temperature, composition and thermal inertia would have allowed the distribution of ices, freshly deposited material and exposed rock to be mapped. These are particularly important for understanding the thermal evolution of a main-belt comet such as 133P.

Sample Return Science In other space missions which perform *in–situ* measurements, the key limitation on the science is the amount of instrumentation that can be deployed, which is limited by mass, power, and data transfer budgets. Instruments must also survive deployment in space and have sufficient sensitivity to achieve their goals. On sample return missions, these issues are not relevant. After returning sample material to Earth, a full suite of scientific methods can be applied, including methods developed after the mission was launched. The analytical techniques that can be applied include SEM-EDX, TEM, Raman, FT-IR, etc., all the way to placing samples in synchrotron beamlines. Laser-based techniques which consume some of the material can also be used. Even ng samples can yield substantial scientific information (Zolensky et al., 2000), as demonstrated by the *Stardust* mission (c.f. Brownlee et al., 2006; Burchell et al., 2009a).

By applying laboratory techniques, a wide range of topics can be studied, including the bulk composition of the samples, mineral paragensis at the μm scale, organic content, any history of thermal or aqueous alteration, whether pre-solar grains are present, and isotopic composition. The NASA *Stardust* mission showed the value of returned samples. The presence of refractory mineral phases in the *Stardust* cometary samples indicated widespread mixing in the proto-solar nebula for example (Brownlee et al., 2006). As well as discrete particles, the *Stardust* aerogel also captured volatiles during its exposure, with a reported detection of glycine (an amino acid) whose D/H ratio suggests it is not a terrestrial contaminant (Elsila et al., 2009). *Stardust* samples analysed at synchrotrons have revealed, amongst other things, details about the elemental composition of samples (Zolensky et al., 2006). The nature of iron oxide grains and their oxidation states have also been revealed (Bridges et al., 2010), permitting comparison to chondritic-porous interplanetary dust particles. This revealed differences between them, indicating a separate origin (Ogliore et al., 2010), and the presence of sub–micron scale calcium-aluminum-rich inclusion—CAIs—in the samples, provided further evidence of widespread mixing in the protosolar nebula (Schmitz et al., 2009).

Other Science In addition to the primary mission goals, there were opportunities for secondary science during the cruise phase. First, the mission would have had the chance to return the first direct samples of main belt asteroid dust, in addition to the main sample of comet dust, as the spacecraft would spend approximately 800 days in the asteroid belt (beyond 2 AU from the Sun). Before and after the rendezvous with 133P, the spacecraft would have traversed the tenuous dust bands that fill the belt, left from past collisions. A separate aerogel sample would have been exposed during this phase, allowing the same Earth–based techniques that would be used for the comet sample to be applied to asteroidal dust. This direct comparison between inner and outer asteroid belt dust, and between asteroid and cometary material, would shed light on the differences between them. This would give a direct measurement of the different mineralogy and D/H ratios in the asteroid belt. A final aerogel sample would have been exposed during the interplanetary cruise phase outside of the asteroid belt, where the spacecraft may have encountered interstellar dust particles.

A full analysis of options based on different orbits was still pending at the time of the proposal, but at least one asteroid was expected to lie close to the trajectory on the way to or from 133P. This would then have been explored by the remote sensing instruments, providing all the science described in the previous sections and adding to our knowledge of asteroids. These instruments would also have taken science and calibration data during Earth and Venus flybys. Finally, the spacecraft, following the return of the capsule to Earth, was expected to have remained on a trajectory that would bring it back to the outer asteroid belt for a potential extended mission to another MBC or asteroid target, where the remote sensing and dust counter instruments would still function.

4. Dust and gas environments of the target main belt comet

The dust density in the tail of 133P was estimated on the basis of the observed properties of the dust. Hsieh et al. (2004) found that the observed dust from 133P is dominated by particles in the 10 μm size range. They measured a dust production rate of $Q_m^{133P} = 0.01$ kg/s, and emission speeds perpendicular to the orbital plane of $v(\beta) = 1.5\sqrt{\beta}$ m/s, where β is the relative strength of radiation pressure and solar gravity. Particles of 10 μm radius have a speed of $v_d = 0.4$ m/s.

Assuming a particle size of 10 μm (mass of 4×10^{-12} kg for a bulk density of 1000 kg m^{-3}), the mass production rate of 0.01 kg/s corresponds to a number production rate of $Q_n = 2 \times 10^9$ s^{-1}. In order to estimate the local density in the tail, we needed to know the speed at which the dust moves along the tail, v_{rp}, and the local cross-section of the tail, w, i.e. the area over which the dust is distributed perpendicular to the tail axis (corresponding roughly to the anti-sunward direction).

The dust moves away from the nucleus because it is accelerated by radiation pressure. For a 10 μm particle at 3 AU from the Sun, this acceleration is $a_{rp} = 4 \times 10^{-5}$ m/s^2, and the speed as a function of nucleus distance, d, is $v_{rp}(d) = \sqrt{2a_{rp}d}$. We assume that—on scales of a few thousand kilometres—the tail diameter increases linearly with the time since emission, t, by $2v_d = 0.8$ m/s. Due to the accelerated motion, the width increases with the square root of the nucleus distance, $w(d) = 2v_d t = 2v_d\sqrt{2d/a_{rp}}$. The spatial density of the dust is given by $\rho_n(d) = Q_n/(\pi/4)/w(d)^2/v_{rp}(d)$. We obtain a number density of 1 m^{-3} for 10 μm particles at 50 km distance from the comet, decreasing with distance as d$^{-1.5}$.

The dust flux on a spacecraft is given by the product of flyby-speed v_{sc} and local dust number density. For $v_{sc} = 5$ km s^{-1}, the flux of 10 μm particles would be 5×10^3 s^{-1} m^{-2}. The total fluence on the spacecraft during the entire fly-by is the integral over the particle number density along the trajectory. A spacecraft passing perpendicularly through the tail at 50 km distance would collect on the order of 4×10^4 m^{-2} grains of 10 μm.

No gas production rate has been measured for 133P, but it is likely that the observed dust production is due to sublimating gas (Hsieh et al., 2004, 2010). We estimate the gas density using two independent approaches, one based on the observed dust speeds, and one assuming a 1:1 dust-to-gas mass ratio. The dust speeds on leaving the coma are proportional to the square root of the gas production rate Q_{gas} (e.g. Müller, 1999). The gas production rate of 133P was inferred by scaling a model of the gas and dust production of comet 67P (Agarwal et al., 2007): $Q_{gas}^{133P}/Q_{gas}^{67P} = (v_d^{133P}/v_d^{67P})^2 = (1.5/900)^2 = 3 \times 10^{-6}$, where the dust emission speeds in the 67P model are given by $v_d^{67P} = 900\ \sqrt{\beta}$ m/s. With $Q_{gas}^{67P} = 10^{28}$ s^{-1}, we find $Q_{gas\ v}^{133P} = 3 \times 10^{22}$ s^{-1}. Assuming a 1:1 dust-to-gas mass ratio, we have $Q_{m,gas}^{133P} = Q_{m,dust}^{133P} = 0.01$ kg/s (Hsieh et al., 2004), which corresponds to a number production rate $Q_{gas\ dtg}^{133P} = 3 \times 10^{23}$ s^{-1}. Combining both approaches we find a likely gas production rate on the order of $Q_{gas}^{133P} = 3 \times 10^{22..23}$s^{-1}, a factor of 10^5 smaller than in the 67P model. For the given level of accuracy, the gas speed is independent of gas production rate and heliocentric distance, hence we divide the 67P coma gas density by 10^5. This gives us a gas number density of 3×10^5 m^{-3} at 50 km from the active area.

To estimate the dust distribution in the tail of 133P, we calculated the positions of dust particles in terms of synchrones (positions of particles of fixed emission date) and syndynes (positions of particles of fixed radiation pressure coefficient β, or size) as introduced by Finson and Probstein (1968) (Fig. 3). We expected that on 17 May 2025, all dust smaller than 10 μm and within 10^5 km of the nucleus would be concentrated within a few degrees of the extended Sun-comet vector, and would have been emitted during the preceding month. On the sunward side of the nucleus, the trajectories of 10 μm particles are likely to turn antisunward at distances as small as 2 km from the nucleus. This strongly suggested that for the successful collection of dust grains, the spacecraft should have been targeted towards a point on the MBC's antisunward side.

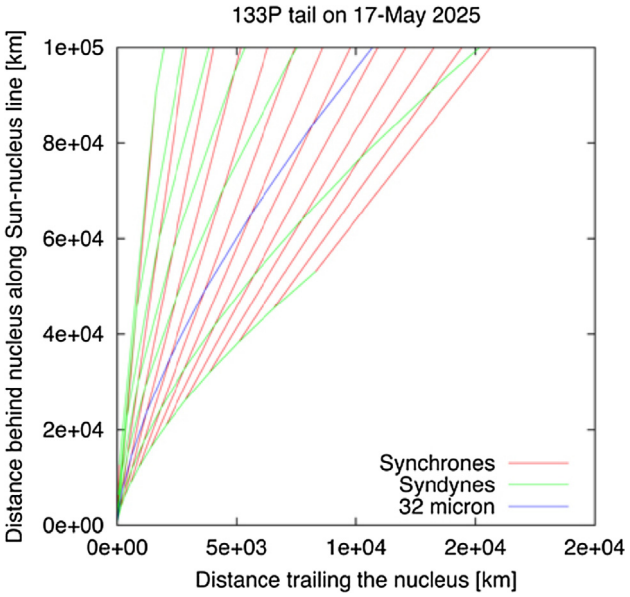

Fig. 3. Syndyne-synchrone map for the tail of 133P on a possible encounter date. Synchrones (red; particles of fixed emission date) and syndynes (particles of fixed radiation pressure coefficient or size), assuming zero emission speed. (Since the speeds in 133P are small, this should be a reasonably good approximation.) The plot is for 17 May 2025, the y-axis is the prolonged Sun-comet vector, and the x-axis is perpendicular to it in the orbital plane. Note the different scales of both axes. The rightmost synchrone corresponds to emission on 10 March. (For interpretation of the references to colour in this figure legend, the reader is referred to the web version of this article.)

5. Mission profile

5.1. Introduction

A 5.4 year mission profile was proposed for *Caroline*, that would allow the encounter between the spacecraft and MBC 133P, during one of the latter's predicted active periods. During the epoch of interest, the active period was expected to extend from May 2024 to June 2025. In defining the mission trajectory, several constraints were imposed:

- an encounter with 133P during its active season
- a launch in 2021–2022 with a mission duration of less than 8 years
- a flyby velocity less than 6 km s^{-1}
- an approach velocity of the sample capsule to Earth of less than 11 km s^{-1}

Under these constraints, a feasible mission scenario was found which could have been further adjusted if required—

the main trade–off being between flyby speed and payload mass, as we expand upon below. More efficient trajectories could have been possible; optimization would have been conducted during the mission study phase.

5.2. Launcher

Launch was to be by Soyuz-Fregat, nominally on November 5, 2021. Of the alternative launchers available, Vega was not perceived as being suitable. Ariane V could clearly launch a more massive, capable spacecraft to an MBC, but was beyond the scope of the M3 mission call. The injection mass versus C3 – the square of the velocity at infinity – was consistent with ESOC analyses for Mars *NEXT*/*Marco Polo* reported at the 2007 Mission Analysis Workshop. No margin on launcher performance was included. An adaptor mass was subtracted from the Soyuz-Fregat injection mass. Direct injection was assumed for the model mission presented in the proposal; use of geostationary transfer orbit, GTO, and a propulsion stage could also be considered. Soyuz-Fregat is restricted in the range of escape declinations it can efficiently access. Therefore where transfers were found with low absolute declinations, consistent with good Soyuz performance, figures with a direct injection to escape orbit are given. In those cases requiring declinations that were difficult or impossible for Soyuz Fregat an assumption can be made that injection is to an equatorial GTO. Escape is then achieved by use of a propulsion module (e.g. similar to the *Lisa-Pathfinder* propulsion module) to achieve the required V_∞ and declination. A generic loss on ΔV to cover finite thrust and plane changing was included in this escape sequence. This propulsion module was then assumed to separate from the remaining spacecraft before subsequent deep space manoeuvres would have been performed.

5.3. Trajectory

Interplanetary trajectory

Fig. 4 shows the proposed interplanetary trajectory, involving a November 2021 launch, followed by Venus and Earth swingbys. An important trade–off in deciding on this profile was between the flyby speed and the payload mass. Due to the much richer potential scientific return anticipated to result from particles captured in aerogel at lower relative velocities, a slow encounter speed was strongly preferred. However, the most efficient trajectory for a slower encounter shifted the encounter date later, to a period when 133P would have been inactive. To ensure a lower speed encounter with an active 133P, extra fuel must therefore have been consumed. As the speed of the flyby under the presented trajectory would have been simply controlled by engine burns a few weeks before and after the encounter, spacecraft mass margins were in reality considerably larger than quoted here because of the possibility of encountering the comet at a higher speed in return for a higher payload mass.

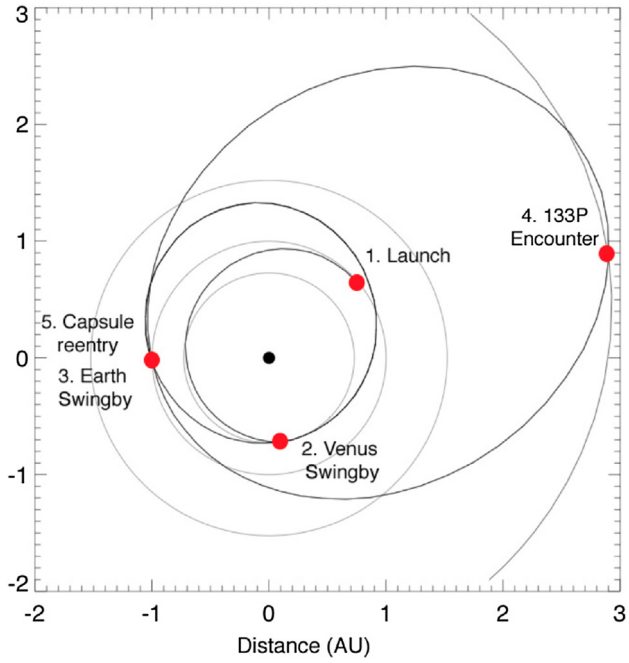

Fig. 4. Venus-Earth transfer after launch in 2021. 133P's orbit has a semi-major axis of 3.16066 AU, eccentricity 0.1623, and inclination 1.4°.

A Venus-Earth-MBC-Earth trajectory was found that achieved these aims (Fig. 4). In case of MBC inactivity, as the region antisunward of the nucleuswas expected to be rich in MBC dust, the closest approach distance should have been increased to maximise the likelihood of dust capture. A generic figure of 100 m/s was added to the deep space manoeuvres to cover fly–bys, dispersion corrections and planet approach navigation. A margin of 5% was added to all manoeuvres, including Earth escape.

Launches in 2021–2022 were considered. Direct injection to escape by Soyuz-Fregat was assumed in all cases, with 5% margin of ΔV and 100 m/s navigation ΔV. A first level trade-off regarding available mass versus fly-by velocity was included. This is a simplistic scenario, the reduction of fly-by velocity performed by two large manoeuvres. In practice, the ΔV penalty for fly-by velocity reduction was expected to be considerably less, using an optimised manoeuvre profile.

The key parameter to be determined was the mass that could have been taken to 133P. Two masses could be considered: The total mass in the targeted state (i.e. returning to Earth in this case), and the "useful" mass in the targeted state. This is total minus the mass associated with the transfer propulsion (e.g. fuel tanks, propulsion elements, associated structure). This measure allows a like for like comparison between mission scenarios (e.g. a high injection mass with a high transfer ΔV/fuel load could result in less useful mass than a lower injection mass with lower transfer fuel load). Therefore the remaining useful mass must include payload, thermal, power, avionics, AOCS, communications. Table 1 shows the maximum Earth-return masses for different flyby speeds. Taking into account a

Table 1
Maximum Earth-return masses for different flyby speeds.

Flyby Speed (m/s)	Mass returning to Earth (kg)	Useful mass Returning to Earth (kg)
5600	1359	1306
4600	696	507
3600	356	99

20% margin, a 4.6 km s^{-1} flyby could have returned a 400 kg useful mass.

Trajectory relative to 133P Due to the expected dust distribution described earlier, *Caroline* would be targeted at a point on the anti-sunward side of the nucleus. To maintain maximum resolution coverage of the nucleus surface with the camera, the closest approach distance would be small; we proposed 50 km as an achievable target through navigation based on ground-based observations of the target and those made from the spacecraft on approach. The trajectory of *Caroline* past the MBC, most simply put as the angle its path would make with the Sun–MBC line, was controlled by the flyby speed. As the dust population forms a narrow tail antisunward of the nucleus, the angle of approach did not have a major effect on the amount of dust collected. We proposed a compromise flyby speed of 4.6 km s^{-1}, which allowed relatively slow capture of dust, a phase angle slighty larger that 90° on approach and slightly less outbound, allowing satisfactory coverage of part of the nucleus surface with the camera, and an attainable slew rate for the remote sensing instruments' periscope around closest approach; at a flyby speed of 4.6 km s^{-1}, a 50 km closest approach distance would have resuled in a periscope rotation rate of ~5°/s.

5.4. Operational mode

The operation of the spacecraft would consist of the following phases:

- Launch (November 5, 2021)
- Instrument commissioning (November 2021-January 2022)
- Venus flyby
- Passive cruise
- Earth flyby
- Passive cruise
- Deployment of aerogel tray
- Extended cruise; aerogel tray rotation for asteroid belt dust capture
- Slowdown burn: start of MBC observations
- Encounter (closest approach on 17 May 2025)
- MBC dust capture phase
- Acceleration burn
- Extended cruise with tray rotated
- Aerogel retrieval into capsule
- Capsule ejection; main bus deflection if fuel margins allowed for possible extended mission
- Entry, descent, and landing of capsule (22 March 2027)

5.5. Mission lifetime

The primary mission would have ended when the sample capsule was safely returned to Earth. The main bus and capsule would have been targeted towards the landing site on Earth, and the capsule released. If fuel reserves allowed, the main bus could then execute a burn to avoid atmospheric entry, in the manner employed by *Mars Express* following the separation of *Beagle–2*, leaving open the possibility of targeting an encounter with a second and even further object(s) following Earth swingby. We did not discuss possible extensions to the primary mission in the proposal, but noted that such extensions were clearly feasible. The mission scenario as presented here would have had a duration of 5.4 years from launch to capsule retrieval.

5.6. Communications requirements

Only occasional communication periods between Earth and spacecraft were foreseen for the extensive cruise phase. During the MBC encounter, a requirement for continuous downlink was foreseen, with an extended period of data return following the encounter itself. Particularly frequent communication periods were also expected during instrument commissioning, the Venus and Earth flybys, target-of-opportunity flybys and around major course correction manoeuvres.

5.7. Alternative trajectories/targets

As mentioned above, alternative routes to 133P were attainable. The spacecraft could also have been targeted at other MBCs. For example, a Venus-Earth-MBC trajectory similar to the one above, with a launch in 2021, could achieve a flyby of 176P/LINEAR in February 2028 with a flyby speed of 6.3 km s^{-1}, and corresponding useful mass returning to Earth of 1405 kg. Lowering the flyby speed to 4.3 km s^{-1} would reduce the returned mass to only 131 kg. The duration of the mission, at 7.4 years, would be considerably longer that the 133P options outlined above. An alternative trajectory to LINEAR included an 8–year long mission, launching in 2022, involving Mars and Earth flybys, with an encounter taking place in December 2028 for a 6.1 km s^{-1} relative speed and 1343 kg useful mass returning to Earth.

Other known MBCs at the time of the proposal were 238P/Read, P/2010 R2 (La Sagra), and P/2008 R1 (Garradd). Mission trajectories to those other potential targets had not been evaluated. A detailed search for suitable trajectories to any potential target with launch in 2020 was not conducted, but it was believed likely that a suitable solution existed.

It was also noted that surveys were being undertaken to identify further MBCs; the real possibility existed at the time of the proposal that even more suitable targets could have been found in the following years.

5.8. Secondary targets

During the spacecraft's extended cruise, we believed that encounters with other small bodies would have been likely to be possible, as demonstrated by the highly valuable target of opportunity asteroid flybys performed by *Rosetta*, *Galileo*, and *Stardust* that in most cases required little additional fuel to achieve. A search for such targets could have been made once a trajectory had been refined.

6. Proposed payload

6.1. Overview of all proposed payload elements

In defining the payload complement, the proposers adhered to an approach that targeted only the mission's core science aims. The scientific instrumentation, of camera, thermal IR spectrometer, and dust counter would be provided by PI-led consortia to be funded by ESA member states and possibly also by international cooperation. In focusing on a core set of instruments, a low mass and relatively low cost mission were achieved. With an awareness of the opportunity to carry further instruments, it was proposed that the expansion of the scientific experiment complement be considered at the mission definition stage. *In situ* attempts at determining the D/H ratio of the MBC volatiles were regarded as an extremely important but highly challenging goal. The inclusion of such an instrument, and other additions to the payload complement, was to be determined in the mission study phase.

It was proposed that the sample return capsule itself be regarded as part of the *Caroline* spacecraft, to be procured and funded by ESA, while the aerogel tray, aerogel cells and possibly other capture material, together with its mechanical delivery arm, be supplied by a PI-led consortium.

6.2. Aerogel capture and sample analysis

Overview and measurement technique The capture of solid particulate matter from a main belt comet was the primary science goal of *Caroline*. A considerable proportion of the spacecraft mass and power resources would therefore have been set aside to ensure successful capture, storage, and return to Earth of the aerogel samples, with redundancy built in, where possible, to ensure that some samples were still returned to Earth in the unlikely event of a mechanical failure in the deployment system.

The spacecraft trajectory past the target MBC would be optimized to ensure the highest success of encountering significant numbers of dust grains, balanced against a desire to keep the relative speed at encounter to a minimum, thus minimizing any detrimental impact effects on the dust grains when collected in the aerogel.

Deployment of the aerogel would be handled by a mechanical arm, based on the instrument arm developed for the *Mars Express Beagle–2* lander. Also deployed would be a matching aerogel sample that would not be exposed to the dust; this would also be returned to Earth and would serve as an essential control for the dust capture experiment. Low power levels around the time of the MBC encounter meant that mechanical activities would have been kept to a minimum around that time. Deployment of the aerogel samples would be monitored by low mass and power camera systems, as very successfully employed on several missions such as *Mars Express*. One aerogel section would have been exposed to asteroidal dust for several years of the mission: when power levels would have allowed, the arm would rotate the sample to maximize exposure to the asteroidal dust stream. The capture system was to be built around SiO_2 aerogel capture cells. Aerogel (Kistler, 1931) is a very porous material, with a bulk density as low as 4 kg m^{-3}. It is a readily manufactured material, available commercially or can be made in a university laboratory. See Burchell et al. (2006) for a history of aerogel, Tsou et al. (2003) for information on the manufacture of *Stardust* aerogel, and Burchell et al. (2009) for an example of how to make samples in a laboratory.

Small particles hitting aerogel at high speed penetrate leaving tracks (Figs. 5 and 6) rather than the craters which occur from impacts in dense media. It has been used as a medium for capturing dust in space since the 1980s (see Burchell et al., 2006 for a review). The dust grains are not captured intact: they undergo heating and shock processing during capture. At 4.5 km s^{-1} impact speed, the peak shot pressures were estimated at 400 MPa in low density (20 kg m^{-3}) aerogel (Trigo-Rodríguez et al., 2008), compared to shocks of typically 45 GPa in normal density materials such as aluminium (Burchell et al., 2009a). Note that the predicted peak pressure in the *Caroline* aerogel impacts were approximately half the value associated with impacts at 6 km s^{-1} (*Stardust*). Despite the impact processing, even in the *Stardust* mission a significant fraction of mineral grains could be found after impact in the tracks in the aerogel, and in the interiors of such grains there

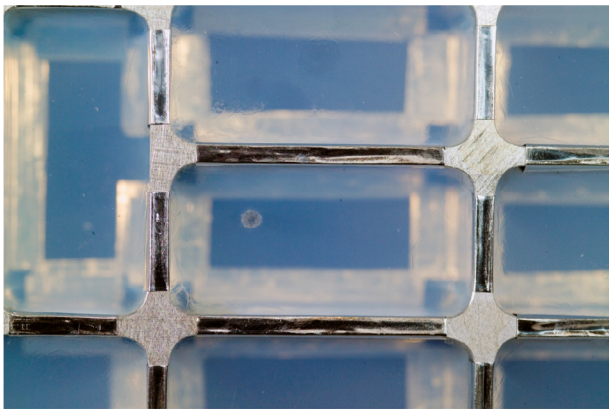

Fig. 5. Closeup view of a cometary impact into aerogel (centre) carried by the *Stardust* Sample Return Canister. Image credit: NASA.

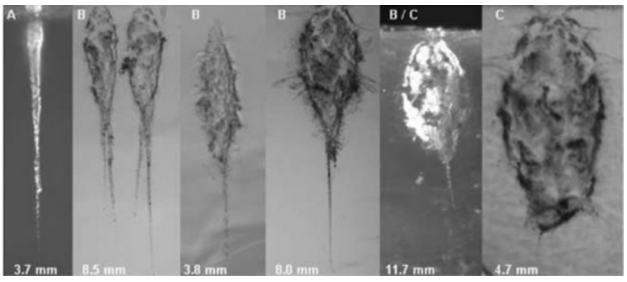

Fig. 6. Example tracks (side view) from cometary dust grains captured in aerogel by the NASA Stardust mission (source: Hörz et al., 2006). Type A tracks are believed to be made by robust, well consolidated grains which are found at the end of the track, Type B tracks are a mixture of well consolidated sub-grains with a finer grained, loosely aggregated component, whilst type C are taken to consist almost totally of fine grained, loosely bound material which ends up distributed over the whole track cavity wall (Trigo-Rodríguez et al., 2008; Kearsley et al., 2009).

can be intact zones with minimal processing. This would have been improved upon for *Caroline*. For example, laboratory tests show that for organic particles with low thermal decomposition temperatures (i.e. worst case scenarios), lowering the encounter speed from 6 km s^{-1} (the *Stardust* speed) to 4.5 km s^{-1} (as here) would have increased the surviving mass fraction from 16% to 49% (Burchell et al., 2009b). This method of dust collection (Tsou et al., 2003) on *Stardust* returned to Earth a cargo of dust with a very high scientific yield (Brownlee et al., 2006; Burchell et al., 2009a).

There are lessons to be learnt from *Stardust* regarding the use of aerogel. For example, whilst very good for capturing mineral grains, capture of organics in aerogel is still less well–understood. There are issues with contamination during manufacture and handling (see Tsou et al., 2003). Thermal modification and ablation during capture can however also present issues, with thin surface coatings lost for example (see Burchell et al., 2009b). *Stardust* did successfully collect indigenous organic material from the comet for analysis on Earth (see Keller et al., 2006; Sandford et al., 2006). However, calibrations would have been needed using aerogel samples made for *Caroline* combined with the impact speed proposed.

After the return, sample analysis would be conducted on Earth in the laboratory. The original particle size distribution could have been obtained and *Stardust* data showed that the aerogel readily collects dust grains at sizes from a few micrometres to mm scale (Hörz et al., 2006; Burchell et al., 2008). Smaller particles are hard to locate in the aerogel, whilst larger ones have the potential to cause severe damage to it. The tracks and individual grains could have been extracted from the aerogel (Westphal et al., 2004; Ishii and Bradley, 2006) and distributed around the world for analysis. The samples could be taken to individual laboratories for SEM-EDX, TEM, laser mass spectrometry, Raman analysis, etc., or taken to central facilities such as synchrotrons. The sample sizes would have been well suited to such analysis and detailed histories of individual grains can be built up (see Zolensky et al., 2000 for details of possible analysis methods of ng scale materials).

Instrument conceptual design and key characteristics

The capture tray would contain a series of small aerogel blocks placed in a grid–like layout. The total aerogel surface area would be of order 1000 cm^2, and the aerogel density would be ~20 kg m^{-3}. By using small aerogel blocks (4 × 2 cm front face and depth of 3 cm), the risk of damage to the aerogel from single, very large impactors would have been confined to individual aerogel blocks. The aerogel thickness of 2 cm was deemed sufficient to capture mm scale impactors at 4.5 km s^{-1} (based on laboratory experiments and the *Stardust* experience). The *Stardust* mission used soft aluminium foil to hold the aerogel in place and by cutting the foil afterwards the aerogel could be removed and each block handled separately if desired. This foil offered an extra collecting surface (about 15% of the area of the aerogel on *Stardust*) which provided craters for studying the sub-μm flux of impactors which are difficult to locate in the aerogel. An extensive set of laboratory experiments has shown that detailed study of the original sub-μm impactors could be made based on the foil craters, where about 1/4 of the impactor could be retained as melted residue at 6 km s^{-1} (Kearsley et al., 2006; Kearsley et al., 2007; Kearsley et al., 2009), with even more retained at the proposed lower *Caroline* encounter speed of 4.5 km s^{-1}. The assembled sample tray complete with aerogel installed, would be vibration tested to ensure it was robust enough to survive launch and re-entry intact.

The arm (Fig. 7) would be a simplified version of the 2.2 kg, 5-degree of freedom anthropomorphic manipulator flown on the *Beagle–2* Mars lander, with the sample tray attached to the wrist. Each joint would comprise a Maxon DC brushed motor and high ratio planetary gearbox, driving through a 100:1 harmonic drive gearbox. Joint position would be detected by a potentiometer mounted directly to the output shaft. The output shaft would rotate in a pair of Kaydon thin section angular contact bearings. The mass-efficient Maxon motor also had heritage from the NASA *Mars Pathfinder* mission. The harmonic drive gearbox offered high torque capability for its size and mass and the thin–section bearings would have a high load capacity

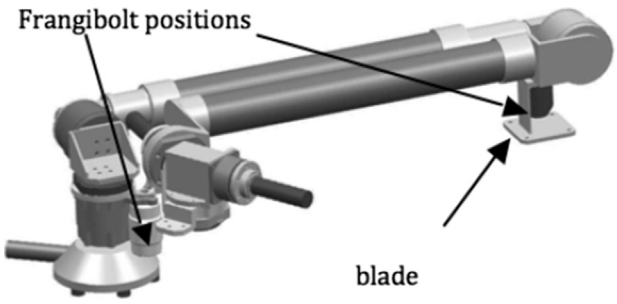

Fig. 7. Beagle–2 arm.

despite their small dimensions. All structural items would be manufactured from titanium in order to closely match the thermal expansion of the bearings, whilst minimising the mass. It is also the best choice where the carbon fibre arm tubes are bonded to the end fittings. Some adaptation of the arm would be required to cope with the thermal environment on *Caroline*. The high launch loads on the arm would be severe and would require it to be held down until required for tray positioning, e.g. with Frangibolts at the elbow and wrist.

Performance assessment with respect to science objectives An extensive suite of laboratory experiments has shown that grains can be captured in aerogel in a form which yields significant chemical, mineralogical and structural information. The *Stardust* mission has shown that this is true for aerogel deployed in space in a fly–by collection mode as proposed for *Caroline*. Details of particle size, mineralogy, D/H ratios, oxidation state etc. could all be obtained.

Resources The *Stardust* model, with 1000 cm^2 of aerogel collector area, was taken as the baseline. A sample canister (SC) would be required, and located inside the sample return capsule (SRC). The SC in *Stardust* was a 61 cm diameter aluminium disk–shaped can, with a height of about 12 cm, with a lower base fixed to the SRC and a lid which opened up to reveal the sample tray (ST). The ST needed an articulated deployment mechanism (a double arm in *Stardust* which was 45 cm long) and at the end of the arm, the aerogel tray itself.

The arm would anchor the ST to the base of the SC, as an example the *Stardust* assembly is shown in Fig. 8. There would be little on-board telemetry or data collection required for the collector. No real-time data concerning the aerogel would be returned to Earth during the encounter. However, monitoring of the SRC and SC would be required to determine that both had opened as required and that the ST has been deployed into position. The operation of the paddle would be monitored with a wide field-of-view "camera on a chip", similar in functionality to the *Mars Express* Visual Monitoring Camera: a low power, very low mass imaging system. The images from this camera would provide a clear picture of the state of the collection paddle without the addition of a set of multiple sensors to the paddle itself. In passing, we note the accessibility that these images would have had to the public. Power would be needed to open the SRC and ST and deploy the articulated arm; the *Beagle–2* arm required 1.2 W for operation.

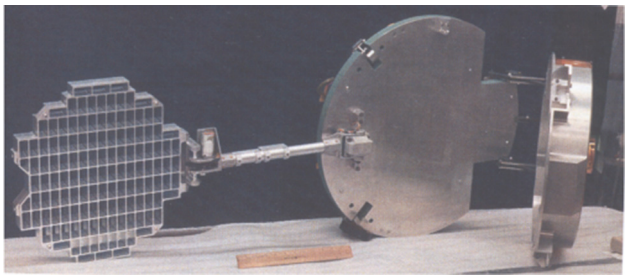

Fig. 8. Stardust aerogel tray ST (left), deployment arm (centre) and sample canister SC (right) which is shown with the arm attached to the SC base with the SC lid open (extreme right). Source: Tsou et al. (2003)

Pointing and alignment requirements and operating modes The aerogel tray would be fixed (via the sample return canister) to the main spacecraft, which would need to be oriented in the correct configuration during the encounter. Given that the encounter speed would be determined by the spacecraft and not by the dust, as long as there would be a viewing geometry which permitted access of the aerogel to the dust, the dust would strike the tray at normal incidence. Some adjustment of the aerogel tray orientation could be provided by the arm.

The collection paddle would be split into sections, to be shielded from impacts at different times. The paddle cover would carry aerogel on both faces. In its unopened state, aerogel would be exposed to asteroid dust during the cruise phase. On approach to the MBC, the lid would open, exposing double the surface area to oncoming dust. The lid face previously exposed to asteroid dust would face away from the oncoming flow during the MBC encounter itself. Approximately one month after the encounter, the lid would again close, again exposing the lid's outer face to oncoming asteroidal dust. It was proposed that at a heliocentric distance of ~2 AU, the sample arm would return the entire paddle to the interior of the return capsule. Some redundancy is included in this design: in the event of the paddle lid being unable to open, the outer face of the lid would be exposed to MBC dust at the time of the encounter.

Specific interface requirements: configuration & thermal needs The aerogel collector would be a passive instrument, and would therefore not need connectors for data or power (beyond the deployment mechanism, see above). It would not be thermally sensitive to variations in temperature at the expected encounter distance from the Sun so would not require any special thermal protection. However, tests have been done on aerogel over the range 175–763 K, and only above 400 K was any change in capture properties found, in that the entrance hole in the aerogel started to narrow, whereas track length did not change until 600 K was exceeded, when it started to shorten (Burchell et al., 2009).

Calibration and other specific requirements There already exists an extensive set of data for performance of aerogel under impact which was made at slightly higher encounter speed (6 km s^{-1}) for *Stardust*. The results are sensitive to impact speed, aerogel density, contaminant levels during manufacture (particularly for sensitive organic analysis, the aerogel could contain organic residues from its manufacture). A set of tests would therefore need to be performed on the mission grade aerogel and aluminium foil to be used here to determine exact, mission specific calibrations. These could have been done in the laboratory with two stage light gas guns. Samples prepared as part of this

could be distributed to laboratories as analogues to test analysis methods. However, the *Stardust* calibration data already showed that the method works successfully.

A small sample of aerogel would have been carried on the spacecraft but not exposed to any dust. This would have provided a control, to ensure that some of the collecting medium would be exposed to the space environment for the same length of time as the collection blocks. Any aerogel retained on Earth for the duration of the mission may have undergone slight changes in its characteristics compared to the space-borne material that could make the investigation of any possible contaminants challenging.

Current heritage and Technology Readiness Level The technology of aerogel capture cells for fly-by is a mature technology. The return capsule technology would need a heat shield and targeting mechanism, but ESA had developed these for other missions (e.g. the *Marco Polo* yellow book), so is not *a priori* an issue.

Critical issues The aerogel manufacture is critical. The quality and contamination control are vital. The aerogel would have needed to be manufactured in advance and stored in dry conditions until use. It would then need to be mounted in the ST. However, all these steps had been performed before for previous missions. A landing site for the sample return capsule needed to be identified and access agreed. The *Stardust* mission landed in Utah, whilst the Japanese Hayabusa asteroid sample return mission landed in Australia. Thus sites are in general available but details of access would have needed to be arranged.

6.3. Visible Camera System, VCS

Description of the measurement technique The mission requirements for the Visible Camera System (VCS) would have been to obtain images of the nucleus of 133P/Elst-Pizarro in the clear filter with a resolution of better than 5 m per pixel, and to map coma structures. The VCS was to be a multispectral imager, optimized to serve both as a scientific and a navigation camera, and based on the Dawn Framing Camera, already in flight at the time of the proposal and operating well on the NASA *Dawn* spacecraft (Fig. 9). The detailed analysis of surface features would include regional variations of albedo, reflectance and spectral ratios of reflectance, and morphological features, including craters and the active region that is the source of the dust coma. The VCS would provide the spatial context for the Thermal Mapping Spectrometer. Together, the data from the two instruments would allow studies of mineralogy. To determine the nucleus bulk density, the volume estimate derived from the shape model as well as the mass of the nucleus would have been required.

Instrument conceptual design and key characteristics The Visible Camera System comprised a refractive lens system, a set of filters with wheel mechanism, a baffle with a door in front of the optics tube, a CCD at the focal plane, a thermal stabilization system, and supporting electronics. The detector data would be read out and processed by a data processing unit. A power converter unit would supply all required power rails for operation and thermal maintenance.

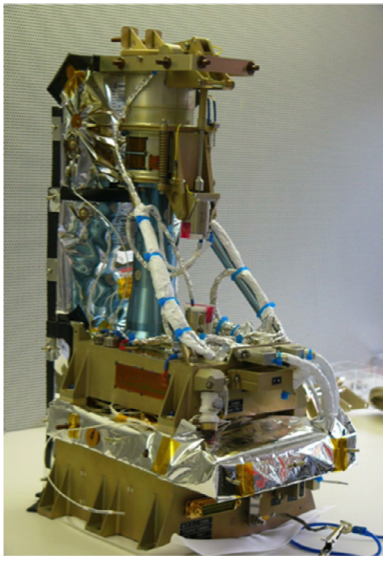

Fig. 9. The *Dawn* framing camera—the basis for the *Caroline* VCS.

Performance assessment with respect to science objectives The flight model would be tested and calibrated extensively before launch, and the results would be verified during the post-launch initial checkout operations. The CCD would employ a lateral anti-blooming gate structure, to prevent photo-generated charge from overexposed regions from spilling over across the columns. The front-side illuminated architecture with semitransparent layers on the detector substrate would further decrease the effective fill factor to about 40–50%, with a peak quantum efficiency of the detector at around 20%. This level of sensitivity would be perfectly adequate to exceed the SNR requirements of the *Caroline* mission. The resolution of the VCS would be up to 5 m per pixel at closest approach (for a CA distance of 50 km), at an angular resolution of 93.7 μrad px^{-1}.

Resources The height of the VCS with its door opened would be 422 mm, and at the base the VCS is 196 mm wide by 215 mm long, including connectors at the front and radiators at the back. The unit would have a mass of 5.5 kg, and an operational power consumption of 17 W.

Visible Camera System instrument control and data processing would be performed by the Data Processing Unit (DPU), which would execute the following general functions:

- Instrument control and monitoring
- Telecommand and telemetry handling
- Acquisition of image data from CCD readout electronics
- Mass storage of acquired image data to decouple image acquisition from image processing
- Housekeeping data acquisition

- Compression of image data (lossless/wavelet)
- On-board image processing
- Execution of imaging sequences

The DPU's minimized resource allocation would be:

- 4.5 to 7 W secondary power consumption for DPU including mass memory
- Mass of 550 g (without housing)
- Board space of 380 cm^2

Images would be natively acquired as raw 16-bit-per-pixel frames. Image acquisition would have several modes. Test pattern, serial readout, storage readout and full-frames would all result in 1092×1056 pixels and define the coordinate system for pixel notation. Cropped acquisitions would have 1024×1024 pixels starting at column 34, row 16. Image acquisition could have been initiated by single or macro command, which contains the requested processing options. To turn the data stream into data products, a set of tools would reconstruct the data as it was onboard, before transmission (raw data reconstruction) and would then transform the raw data into physical values for scientific evaluation (calibration).

Pointing and alignment requirements The tracking of the nucleus during closest approach would be achieved using a periscope that could rotate to keep the target in the VCS field of view, while maintaining a fixed spacecraft attitude to keep the dust shields in the ram direction and the aerogel sample holder aligned correctly.

Operating modes The VCS would operate in science and in calibration modes, with the outer door open or closed.

Specific interface requirements A set of integrated sensors and heaters would be under spacecraft control, and radiators for cooling would have been required for thermal control. The CCD sensor would have to operate at a stable temperature of −60°C or below.

Calibration and other specific requirements There would have been various calibration methods, such as camera calibration, ground calibration and inflight calibration. The VCS would observe the standard stars 51 Pegasi, Vega, 20 Cephei, 42 Pegasi, and 73 Ceti, and suitable planets, as calibration targets. The calibration lamp would be a set of six AlGaInP light-emitting diodes attached to the top flange of the objective barrel. The lamp would illuminate the inner face of the front door through a sequence of pulses on the 5.2 V line. The emission spectrum would be asymmetric, peaking at approximately 635 nm, with half maxima at 614 and 660 nm.

Current heritage and Technology Readiness Level The VCS would have been an exact copy of the Dawn Framing Camera, the German contribution to the NASA *Dawn* mission, which is flight proven. Depending on the results of the detailed analysis of possible orbits and close approach parameters, some adjustments to the optical design could have been made to optimise the pixel scale and FOV for *Caroline*.

6.4. Thermal Mapping Spectrometer: TMS

Instrument Measurement Technique This instrument would have been an imaging Fourier transform mapping spectrometer utilising a beam- shearing interferometer to generate a set of spatially resolved interferograms to be imaged onto a detector array. This would allow spectral image cubes of the target body to be measured. The instrument would cover the key spectral range of 400–2000 cm^{-1} (5–25 μm) with a maximum programmable resolution of 10 cm^{-1}. The extended spectral range was considered vital, as it includes important diagnostic mineral absorption bands as well as the thermal continuum due to the full diurnal temperature range of the MBC, as described in the science objectives.

Instrument design The proposed instrument (Fig. 10) was at the time the latest in a series of interferometers designed by F. Reininger of SpiLab, breadboarded at SpiLab and JPL, with a version designed to be integrated with cold optics and detectors assembled and tested at the University of Oxford. The instrument would use a mid-infrared beam splitter and all reflective optics to image the interferogram on to a 640 × 480 uncooled micro-bolometer array, rather than using a traditional moving mirror arrangement. The mirrors would be fabricated from aluminium alloy and incorporated into their mounts.

This design led to a highly reliable, compact *f*/4, low mass and low power instrument with no moving parts except a rotary scan/calibration mirror assembly. The scan mirror would be essential to allow measurements of space and of a low power miniature black body target to maintain radiometric calibration during operation. The rotation axis of this scanning mirror would be oriented so that a single mechanism could perform this calibration as well as scanning the field of view across the object. In the case of *Caroline*, the instrument entrance aperture would be baffled and shuttered to prevent contamination during periods of closest approach and with the scan/calibration mirror and blackbody calibration target likely to be mounted external to the main body of the instrument in a separate periscope.

Physical resources and interfaces to spacecraft The instrument would have needed a minimum of four fixation points. Instrument alignment, if practical, should have been such that the scan mirror would rotate the field of view across the direction of peak surface motion caused by rotation or spacecraft motion. The 6 kg instrument would have operated at ~10 W.

Operations and calibration procedures The image cube generated by the instrument is illustrated in Fig. 11. The target would be mapped by scanning the 480 cross track pixels across the surface. To maximise signal to noise, the measurements along the 640 pixel axis would not correspond to the same point on the target. Instead, these would be scanned to assemble the interferogram of each single point.

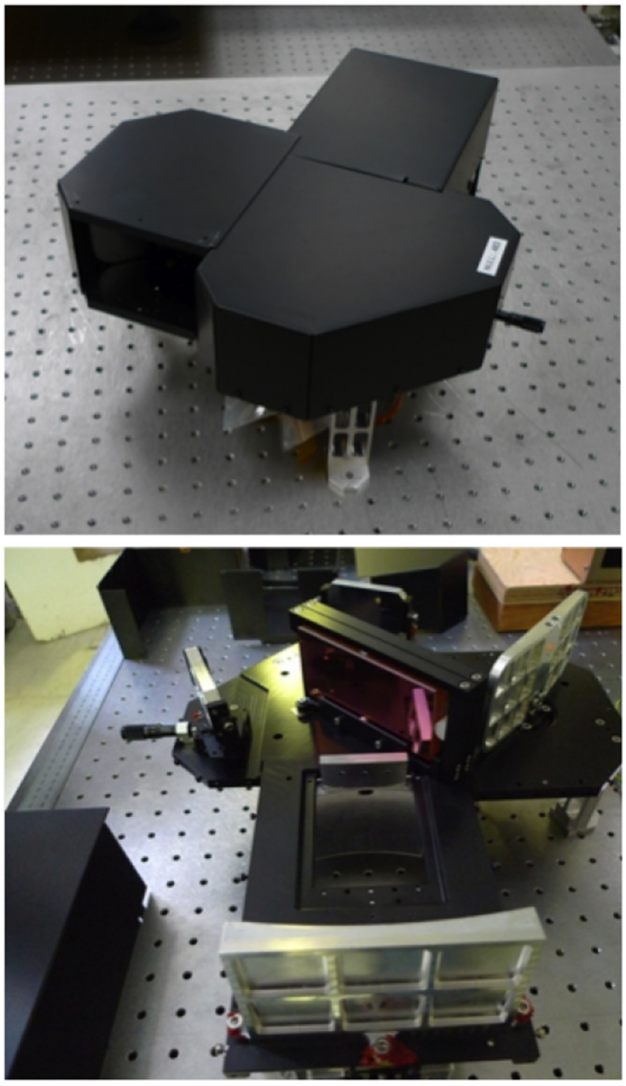

Fig. 10. TMS instrument breadboard showing scan mirror and beam splitter. Credit: SPIlab Inc./University of Oxford.

The instrument design is ideally suited to a "pushbroom" measurement approach in which the motion of the spacecraft around the target body would provide the scanning to build up the interferograms, but would include a micro-stepping rotary mechanism to step along the scan direction in cases where orbit geometry or object motion do not allow this. The nominal operating mode is illustrated in Fig. 12.

Black body views at the start and end of the scans would allow each observation sequence to include all information needed for calibration. Data would be averaged within the instrument differently for the two axes of the array. Averaging across the track (the spatial dimension) would be determined by the desired resolution. Along the 640 pixel dimensions, 3 points would normally be averaged since only 210 samples would be needed to achieve the desired spectral resolution. The instrument would include the capability of excluding any bad pixels. In addition, each sample would be averaged in time to match the scan rate and spatial resolution. The data volume returned to Earth would thus be determined by the programmed resolution, not by the potential data rate produced by the array.

6.5. Dust counter

The mission's primary goal would have been to return MBC dust to Earth, where dust particles could be analyzed with cutting-edge techniques. Given limited mass and power availability on the spacecraft, we believed that the resources that would be required for the comprehensive *in situ* analysis of dust would instead be best invested in securing the successful return of the dust sample. However, contextual information on the dust populations encountered would still ideally be needed.

We therefore proposed that a dust counter be employed on one or more of the dust shields to monitor the timing of impacts and the approximate size distribution of dust. Such an instrument, employing several techniques including diaphragm-mounted piezo-electric detectors, was very successfully employed on the *Giotto* mission to comets 1P/Halley and 26P/Grigg-Skjellerup (McDonnell et al., 1987). Using the *Giotto* Dust Impact Detector as a guide, we anticipated that the mass required would be 3 kg, power 2 W.

6.6. In situ mass spectroscopy

In situ measurement of the D/H isotope ratio of the body's volatiles would have been an extremely valuable observation. However, given the very low gas production rate of 133P, the neutral coma surrounding the object was likely to have been extremely tenuous. Due to the com-

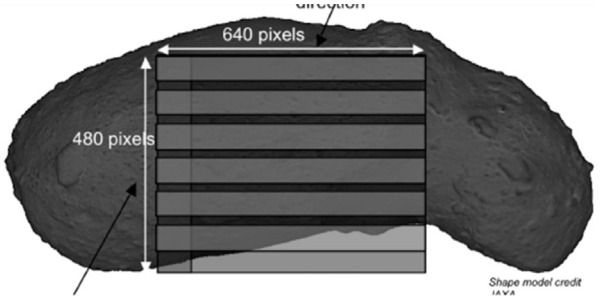

Fig. 11. Scanning pattern of the TMS instrument.

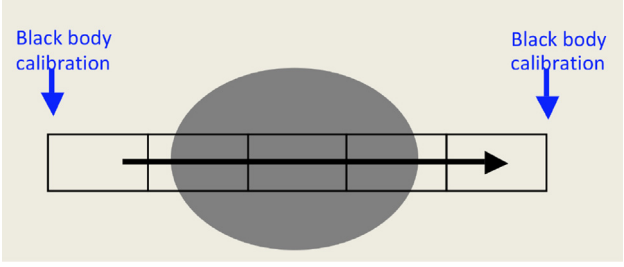

Fig. 12. TMS nominal scanning mode.

bined low gas production rate and relatively large heliocentric distance at the time of encounter, D/H ratio-determining experiments based around UV, near-IR, or submillimetre spectrometers were believed by the proposers to be unlikely to be capable of making this measurement due to the high wavelength resolution and relatively large abundance of OH/H_2O required.

In situ measurement of the coma gases is another potential technique for determining the D/H ratio of the MBC volatiles, and previously successfully demonstrated at 1P/Halley. It may have been possible for a dedicated instrument to detect and measure the gases within the coma, with the aim of measuring the isotope ratios of the volatiles, however, given that the estimates of the production rate resulting from our modeling were very low, at $\sim 10^{23}$ molec s^{-1}, significant resources could have been put into a sophisticated instrument that may not have encountered enough material to make a measurement. Countering this argument was the fact that *Caroline*'s presence at an MBC would be an opportunity to attempt to make a unique and ground-breaking observation. Given the extreme challenges of making the measurement of D/H, we therefore defered a final decision on whether to include a suitable instrument to the mission definition stage, and did not include it in the model payload presented in the proposal.

It was however suggested that a compromise solution would be a low–mass, low–power instrument that would have the capability of measuring the D/H ratio if the gas number density was high enough, but would also return other extremely valuable scientific information on the MBC even in the event of the D/H measurement being unsuccessful. Due to the very low particle densities, an instrument with a high geometric factor was a key requirement. Existing instruments do not meet this. The geometric factor could be increased by enlarging the instrument but this would have had a major impact on the mass. On the other hand, by optimising the instrument performance to focus primarily on extracting just the H/D and/or the H_2O/HDO ratios, the impact of the increased mass could have been significantly reduced. Such a highly miniaturised mass analyser was then under development at MSSL, optimised for mass analysis of cold ions in the Earth's upper atmosphere. A proof-of-concept analyser (Fig. 13) had been fabricated and tested. Based on results from this device, a proto-flight model was then being developed for TechDemoSat, UKTDS (which later successfully returned data for low Earth orbit).

The complete instrument including the detector and electronics was expected to weigh less than 0.5 kg. The study would also look into adapting and optimising this instrument for *Caroline*, as a Miniaturised Instrument for Neutral and Ion Mass, MINIM. The scientific return of an ion-detecting instrument would be further enhanced by the inclusion of a low-resource magnetometer, which would provide pitch angle information and hence the direction of arrival of ions at the instrument, together with valuable data on the interaction between the heliospheric magnetic field and the MBC, and the possible presence of ion pickup-generated waves. A low resource magnetoresistive (MR) array, as was being developed by Imperial College, could have achieved this. A four sensor MR implementation would have a mass of ~0.3 kg; these sensors could have been body-mounted, or sited on a ~1 kg boom to address magnetic cleanliness issues.

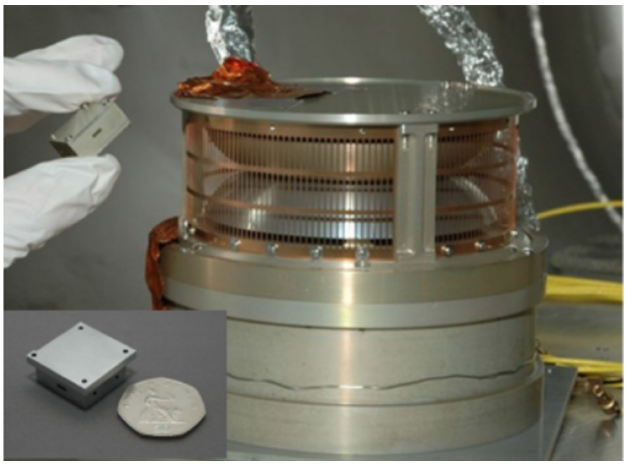

Fig. 13. A proof-of-concept analyser, in gloved hand, alongside MSSL's conventional, state of the art top-hat type Improved Plasma Analyser, has been fabricated and tested.

The proposed core payload is summarized in Table 2. Note that systems associated with the sample return capsule, as well as the capsule itself, are not included in the table and are described in the next section.

7. System and key spacecraft requirements

Several parameters drove the design of the spacecraft systems; these were: reliable dust capture and safe return to Earth, protection of the spacecraft from dust impacts, accurate targeting to sample sufficient amounts of MBC dust, and the provision of power.

Caroline would have been a three-axis stabilized spacecraft, controlled by thrusters. Its attitude would be guided by two requirements: the sample collection device would need to be oriented in a direction where it presented a maximum cross-section to oncoming dust during the MBC encounter, and also during the cruise phase to collect asteroid dust. Also, given its planned operation at over 3 AU from the Sun, for maximum efficiency, its solar panels would ideally need to be oriented normal to the sunward direction. We envisaged the encounter taking place with direct downlink of data to Earth via the HGA, which provided another constraint on attitude. Although the dust grains that we expect to encounter would have been low in mass, there existed a real risk that torques applied by impacts of more massive particle could affect the spacecraft attitude during the encounter phase. Active attitude con-

Table 2
Summary of proposed core Payload.

Instrument	Mass (kg)	Power (W)	Data volume for whole mission	TRL at submission
Aerogel sample handling system	7 (2.2 of this for arm)	2	N/A	3
Visible Camera System + DPU	5.5 + 0.55	17 + (4.5–7)	2500 Mbyte	9
Thermal Infrared Spectrometer	3.0	2–3.5	1500 Mbyte	4
Dust Counter	3.0	2	10 Mbyte	3
Total	19.05	31.5	4010 Mbyte	–

trol with autonomous real-time corrections would be required during the encounter itself, for several reasons:

- spacecraft safety, to ensure that the dust shield was correctly oriented to protect the main bus
- Aerogel sampling, to keep the sample tray oriented as close as possible to normal to the oncoming dust to maximize its collecting area
- Pointing of the remote sensing instruments, to ensure that the nucleus remained in the field of view around closest approach, and to minimize motion blur in imaging data
- Pointing of the HGA to Earth for live data transmission; as all flyby data would be recorded for further playback post-encounter, this constraint was not as tight as the others

This autonomous AOCS system would have required a significant software and engineering development effort. Imaging data would likely need to have been combined with information from attitude sensors to keep the spacecraft orientation fixed, and the remote sensing periscope slew speed may also have needed to be partially controlled by live information from the AOCS. Intelligent recognition of the nucleus location in images would in turn help guide the AOCS system.

At the end of the primary mission, the mated primary spacecraft and capsule would have been targeted for Earth atmosphere entry as soon as possible prior to arrival at Earth. A failsafe, timer-based capsule detachment sequence would have ensured that, in the event of loss of command of the spacecraft pre-release, the capsule would still have a chance of returning to Earth. On release, the return capsule would be spun up through the use of curved guiderails to ensure its stability for atmospheric re-entry at Earth. Following release, the main spacecraft would perform a trajectory correction maneuver to avoid entry into Earth's atmosphere and, if sufficient fuel remained, to travel on to a secondary target. The sample return capsule would employ an accelerometer to detect atmospheric entry and to release its parachute at the correct time. It would also be armed with failsafe timer for parachute release, programmed prior to Earth return.

For the extended cruise phases, little data would be returned to Earth. The encounter period would have been very intense, and we proposed that for redundancy, all data were stored on board for later playback as well as being downlinked directly. This would have ensured that data would be returned even in the unfortunate event of the spacecraft being lost, or transmission being interrupted during the flyby by, e.g. large dust impact.

This mission would require the use of deep space antennae, e.g. New Norcia. As the spacecraft would always be near the ecliptic plane, ground stations in both hemispheres could have been used.

Total payload mass would have been 19 kg, consuming 31.5 W peak. We estimated that around 40 W would be required for thermal control. Taking into account the return capsule and its associated holder and release system, solar panels, lightweight dust shields, main bus, antennae, AOCS and thermal control system, we estimated a total dry spacecraft mass of approximately 250 kg. Given the possibility of returning up to ~400 kg to Earth at our chosen flyby velocity, we believed that this demonstrated sufficient scope to either enhance the scientific payload if required, or to carry more fuel with a view to extending the mission following the delivery of the samples to Earth.

The spacecraft would operate over a range of heliocentric distances from 0.68 to 3.22 AU, i.e. under solar insolation levels ranging from 9.7% to 216% of that at 1 AU. This would complicate the thermal design due to the wide temperature range that the spacecraft would have experienced.

Basic Spacecraft Concept Given the above drivers, we proposed an initial spacecraft concept designed around a main spacecraft bus, employing solar panels which would unfold into a single plane following launch. During the MBC encounter, the local dust ram direction would be almost parallel to the plane of the solar panels. One solar panel edge and the main bus would be protected from dust impacts by a metallic shield separated by several cm from Kevlar blanketing. The shield would be wide enough to protect the spacecraft from direct impact even if the bus was tilted up to 5° from the nominal attitude due to torques imparted by high velocity dust grains. To the metallic shield would be attached a piezo-electric dust counter to monitor impact flux during the MBC encounter. The remote observation instruments would be housed within the main bus, and would have viewed their target either via a single, shared periscope system, or individual rotating periscopes to provide some redundancy. The mass spectrometer, if included, would have an aperture oriented to sample the local ram direction at the MBC. The sample return capsule itself would be shielded from particle impact, but the sample tray would have been exposed to

the dust. Communications between the spacecraft and Earth would be facilitated by both high and low gain antennae. The sample return capsule would be attached to the bus face oriented away from dust ram, next to which would be placed the sample control arm. Some steering of the HGA would be highly beneficial, in a plane parallel to the ecliptic.

This design would provide a compact spacecraft employing efficient use of mass. The payload mass, excluding sample return capsule, would constitute approximately 10% of the total dry mass. The design of the sample return capsule would be guided by experience gained through the *Huygens* and *Beagle–2* heritage. Other agencies' experience with similar interplanetary sample return missions such as *Genesis*, *Stardust*, and *Hayabusa*, clearly demonstrated the feasibility of this sample return technique. We expected the capsule to also build upon design exercises linked to the original *Marco Polo* studies.

Remote sensing periscope Tracking of the nucleus would be achieved through the use of a periscope, within which would be mounted a front-silvered flat mirror inclined at 45° to the optical axis. The entire periscope assembly would rotate about an axis parallel to the main optical axis of the remote sensing instruments, and would provide those instruments with a view of the target unobscured by the spacecraft dust shield. The use of a rotating periscope would allow the spacecraft to maintain full three axis stabilization during the flyby, minimizing the amount of dust shielding required. Possible frosting of the mirror by dust impacts during approach to the target was a recognized risk, partially alleviated by the proposed addition of a baffle around the mirror.

If the spacecraft was targeted especially close to the nucleus, the periscope would have needed to execute almost full 180° rotation to allow imaging of the object during the entire encounter period. A close flyby would incur a complication in the form of very rapid motion of the nucleus across the camera's field of view around closest approach; rapid periscope rotation would therefore also be a requirement. Active tracking of the nucleus by onboard software would allow good coverage of the target to be maintained throughout the encounter, and, if required, further small adjustments could have been made in pointing through the rotation of the spacecraft about the ram direction axis—this would not affect the angle that the aerogel sample would have presented to the oncoming dust.

Alternative approaches to the use of a periscope included full rotation of the spacecraft to track the target. This would however radically increase the amount of spacecraft shielding required, and would be incompatible with the strong desire to keep the aerogel sample oriented perpendicular to the ram direction. This could be compensated by rotating the aerogel sample during flyby to counteract spacecraft attitude changes, however, the risk involved in performing such an operation at a critical point in the mission was best avoided. The final alternative was to mount the remote sensing instruments on a steerable scan platform. This would introduce significant additional mass to the spacecraft, and would still not allow observations of the target prior to closest approach without introducing a periscope into the design.

Sample Return Capsule A vital component of the mission would have been the sample return capsule. A minimum mass for the capsule of approximately 50 kg was estimated, and a similar mass assigned to the capsule support systems, release mechanism, release guiderails, etc. As well as housing the sample tray, the capsule would accommodate a parachute and associated release mechanisms, and possibly also a battery-powered radio beacon. It was noted that significant study work for high speed entry capsules had already been carried out as part of the *Marco Polo* mission study, and ESA heritage in this area was clearly demonstrated by the *Huygens* probe. Collaboration with sample return studies as part of the ESA Aurora programme was also to be considered. Housing of the aerogel sample tray inside the capsule could have had a significant impact on the capsule design. As the tray would be designed to maximize surface area, its flat shape would need to be accommodated, or its design made significantly more complex to allow folding into the capsule. As the sample tray and arm would be provided by a PI-led team, the interface between this sample delivery system and the capsule itself would need significant coordination. It was proposed that the sample delivery arm be mounted to the main spacecraft bus rather that to the inside of the capsule.

Capsule Recovery and Aerogel Handling Capsule recovery operations were expected to require significant resources, requiring a ground team to coordinate and collect the capsule from what may have been a very remote area. The recovered capsule would be returned to a mobile cleanroom for initial condition assessment, followed by boxing for safe transportation to the mission's primary analysis laboratory. The capsule's backshell and heatshield, which may have separated from the capsule itself before landing (to be confirmed during detailed mission design), would also be recovered for scientific and technical analysis.

The provision of a central cleanroom suitable for the initial assessment, archiving, and distribution of aerogel samples would need to be decided upon. This activity could have been done in parallel with similar studies into the analysis of martian sample return, which at the time of the proposal was anticipated to also occur in the late 2020s. The costs of such a facility were not included in the *Caroline* proposal. If the cleanroom would not be used for sample analysis itself, then the resources required for a sample distribution effort could have been relatively modest.

Spacecraft Cleanliness As the MBC dust samples would undergo intense scrutiny, the aerogel blocks within which they would be contained would need to be handled in an extremely clean environment, to avoid contamination. Surfaces to which the aerogel may have been exposed, in and around the capsule and sample delivery arm, would also need to be kept contaminant-free. With the proposed core

Fig. 14. The sample return capsule from NASA's *Stardust* mission successfully landed at the U.S. Air Force's Utah Test and Training Range in Dugway, Utah on January 15, 2006. Image credit: NASA.

payload, there would have been no requirement for strict magnetic cleanliness issues that could have arisen if a magnetometer was included. However, standard testing for EM interference of experimental data by spacecraft systems would have been required.

8. Discussion and conclusions

Ultimately *Caroline* was not selected by ESA for further study following the M3 call for mission proposals. Many of the proposing team were subsequently involved in an alternative MBC mission proposal for the M4 and M5 calls, *Castalia*, which is described elsewhere in this issue (Snodgrass et al., 2018). Instead of a sample return mission, *Castalia* proposes to take a more comprehensive *in situ* analysis payload to rendezvous with 133P, a mission more analogous to *Rosetta* than *Stardust*, although still on an M-class scale. There are a number of advantages or disadvantages to the two different approaches: Sample return remains the 'holy grail' of planetary exploration, due to the vastly superior array of techniques that can be applied in laboratories on Earth. However, the primary science driver of an MBC mission is measuring the volatile (ice) component, and isotopic ratios in this, which is not included in returned dust samples. While hydrated mineral samples returned by *Caroline* would have pointed towards the D/H ratio in water in 133P, sampling of the escaping water vapour is a more direct measurement. As discussed above, it is difficult (likely impossible with current technology) to collect enough of the diffuse gas coma of an MBC during a fast flyby, so instead of a return trajectory a rendezvous and extended sampling period is necessary for this approach. Although an extended stay at the MBC is also advantageous for remote sensing, the mission duration is relatively long, compared to *Caroline*, and there is no possibility to return to Earth afterwards with a sample for more detailed analysis. Since *Caroline* was proposed, two further near-Earth asteroid sample return missions have been launched (NASA's *OSIRIS-Rex* and JAXA's *Hayabusa-2*), but at the time of this writing, no sample return mission from beyond near-Earth space has been selected by any agency. For the study of mineralogy in the asteroid belt, *Caroline*'s proposed sample return remains a convincing concept, and likely the most reasonable way to obtain very detailed information on these bodies. The recent success of the *Rosina* mass spectrometer on *Rosetta* (Altwegg et al., 2015) suggests that study of volatiles like water is best approached *in situ* (Fig. 14).

Acknowledgments

GHJ is grateful to the UK Science and Technology Facilities Council (STFC) for partial support through consolidated grant ST/N000722/1. CS is funded by STFC through an Ernest Rutherford fellowship.

References

Agarwal, J., Müller, M., Grün, E., 2007. Dust environment modelling of Comet 67P/Churyumov-Gerasimenko. Space Sci. Rev. 128, 79–131. https://doi.org/10.1007/s11214-006-9139-1.

A'Hearn, M.F., Belton, M.J.S., Delamere, W.A., Feaga, L.M., Hampton, D., Kissel, J., Klaasen, K.P., McFadden, L.A., Meech, K.J., Melosh, H.J., Schultz, P.H., Sunshine, J.M., Thomas, P.C., Veverka, J., Wellnitz, D.D., Yeomans, D.K., Besse, S., Bodewits, D., Bowling, T. J., Carcich, B.T., Collins, S.M., Farnham, T.L., Groussin, O., Hermalyn, B., Kelley, M.S., Kelley, M.S., Li, J.Y., Lindler, D.J., Lisse, C.M., McLaughlin, S.A., Merlin, F., Protopapa, S., Richardson, J.E., Williams, J.L., 2011. EPOXI at Comet Hartley 2. Science 332, 1396–1400. https://doi.org/10.1126/science.1204054.

A'Hearn, M.F., Belton, M.J.S., Delamere, W.A., Kissel, J., Klaasen, K.P., McFadden, L.A., Meech, K.J., Melosh, H.J., Schultz, P.H., Sunshine, J.M., Thomas, P.C., Veverka, J., Yeomans, D.K., Baca, M.W., Busko, I., Crockett, C.J., Collins, S.M., Desnoyer, M., Eberhardy, C.A., Ernst, C.M., Farnham, T.L., Feaga, L., Groussin, O., Hampton, D., Ipatov, S.I., Li, J.Y., Lindler, D., Lisse, C.M., Mastrodemos, N., Owen, W.M., Richardson, J.E., Wellnitz, D.D., White, R.L., 2005. Deep Impact: excavating Comet Tempel 1. Science 310, 258–264. https://doi.org/10.1126/science.1118923.

Altwegg, K., Balsiger, H., Bar-Nun, A., Berthelier, J.J., Bieler, A., Bochsler, P., Briois, C., Calmonte, U., Combi, M., De Keyser, J., Eberhardt, P., Fiethe, B., Fuselier, S., Gasc, S., Gombosi, T.I., Hansen, K.C., Hässig, M., Jäckel, A., Kopp, E., Korth, A., LeRoy, L., Mall, U., Marty, B., Mousis, O., Neefs, E., Owen, T., Rème, H., Rubin, M., Sémon, T., Tzou, C.Y., Waite, H., Wurz, P., 2015. 67P/Churyumov-Gerasimenko, a Jupiter family comet with a high D/H ratio. Science 347, A387. https://doi.org/10.1126/science.1261952.

Bagnulo, S., Tozzi, G.P., Boehnhardt, H., Vincent, J.B., Muinonen, K., 2010. Polarimetry and photometry of the peculiar main-belt object 7968 = 133P/Elst-Pizarro. Astron. Astroph. 514, A99. https://doi.org/10.1051/0004-6361/200913339.

Balsiger, H., Altwegg, K., Geiss, J., 1995. D/H and O-18/O-16 ratio in the hydronium ion and in neutral water from in situ ion measurements in comet Halley. J. Geophys. Res. 100, 5827–5834. https://doi.org/10.1029/94JA02936.

Bandfield, J.L., 2007. High-resolution subsurface water-ice distributions on Mars. Nature 447, 64–67. https://doi.org/10.1038/nature05781.

Barucci, M.A., Doressoundiram, A., Fulchignoni, M., Florczak, M., Lazzarin, M., Angeli, C., Lazzaro, D., 1998. Search for aqueously altered materials on asteroids. Icarus 132, 388–396. https://doi.org/10.1006/icar.1998.5889.

Beck, P., Quirico, E., Sevestre, D., Montes-Hernandez, G., Pommerol, A., Schmitt, B., 2011. Goethite as an alternative origin of the 3.1 μm band on dark asteroids. Astron. Astroph. 526, A85. https://doi.org/10.1051/0004-6361/201015851.

Bockelée-Morvan, D., Gautier, D., Lis, D.C., Young, K., Keene, J., Phillips, T., Owen, T., Crovisier, J., Goldsmith, P.F., Bergin, E.A., Despois, D., Wootten, A., 1998. Deuterated water in Comet C/1996 B2 (Hyakutake) and its implications for the origin of comets. Icarus 133, 147–162. https://doi.org/10.1006/icar.1998.5916.

Boss, A.P., 1998. Temperatures in protoplanetary disks. Annu. Rev. Earth Planet. Sci. 26, 53–80. https://doi.org/10.1146/annurev.earth.26.1.53.

Bridges, J.C., Burchell, M.J., Changela, H.C., Foster, N.J., Creighton, J. A., Carpenter, J.D., Gurman, S.J., Franchi, I.A., Busemann, H., 2010. Iron oxides in comet 81P/Wild 2. Meteoritics Planet. Sci. 45, 55–72. https://doi.org/10.1111/j.1945-5100.2009.01005.x.

Brownlee, D., Tsou, P., Aléon, J., Alexander, C.M.O.., Araki, T., Bajt, S., Baratta, G.A., Bastien, R., Bland, P., Bleuet, P., Borg, J., Bradley, J.P., Brearley, A., Brenker, F., Brennan, S., Bridges, J.C., Browning, N.D., Brucato, J.R., Bullock, E., Burchell, M.J., Busemann, H., Butterworth, A., Chaussidon, M., Cheuvront, A., Chi, M., Cintala, M.J., Clark, B. C., Clemett, S.J., Cody, G., Colangeli, L., Cooper, G., Cordier, P., Daghlian, C., Dai, Z., D'Hendecourt, L., Djouadi, Z., Dominguez, G., Duxbury, T., Dworkin, J.P., Ebel, D.S., Economou, T.E., Fakra, S., Fairey, S.A.J., Fallon, S., Ferrini, G., Ferroir, T., Fleckenstein, H., Floss, C., Flynn, G., Franchi, I.A., Fries, M., Gainsforth, Z., Gallien, J.P., Genge, M., Gilles, M.K., Gillet, P., Gilmour, J., Glavin, D.P., Gounelle, M., Grady, M.M., Graham, G.A., Grant, P.G., Green, S.F., Grossemy, F., Grossman, L., Grossman, J.N., Guan, Y., Hagiya, K., Harvey, R., Heck, P., Herzog, G.F., Hoppe, P., Hörz, F., Huth, J., Hutcheon, I.D., Ignatyev, K., Ishii, H., Ito, M., Jacob, D., Jacobsen, C., Jacobsen, S., Jones, S., Joswiak, D., Jurewicz, A., Kearsley, A.T., Keller, L.P., Khodja, H., Kilcoyne, A.L.D., Kissel, J., Krot, A., Langenhorst, F., Lanzirotti, A., Le, L., Leshin, L.A., Leitner, J., Lemelle, L., Leroux, H., Liu, M.C., Luening, K., Lyon, I., MacPherson, G., Marcus, M.A., Marhas, K., Marty, B., Matrajt, G., McKeegan, K., Meibom, A., Mennella, V., Messenger, K., Messenger, S., Mikouchi, T., Mostefaoui, S., Nakamura, T., Nakano, T., Newville, M., Nittler, L.R., Ohnishi, I., Ohsumi, K., Okudaira, K., Papanastassiou, D.A., Palma, R., Palumbo, M.E., Pepin, R.O., Perkins, D., Perronnet, M., Pianetta, P., Rao, W., Rietmeijer, F.J. M., Robert, F., Rost, D., Rotundi, A., Ryan, R., Sandford, S.A., Schwandt, C.S., See, T.H., Schlutter, D., Sheffield-Parker, J., Simionovici, A., Simon, S., Sitnitsky, I., Snead, C.J., Spencer, M.K., Stadermann, F.J., Steele, A., Stephan, T., Stroud, R., Susini, J., Sutton, S.R., Suzuki, Y., 2006. Comet 81P/Wild 2 Under a Microscope. Science 314, 1711. doi:https://doi.org/10.1126/science.1135840.

Burchell, M., Fairey, S., Foster, N., Cole, M., 2009. Hypervelocity capture of particles in aerogel: dependence on aerogel properties. Planet. Space Sci. 57, 58–70. https://doi.org/10.1016/j.pss.2008.11.004.

Burchell, M.J., Fairey, S.A.J., Foster, N.J., Cole, M.J., 2009a. Hypervelocity capture of particles in aerogel: dependence on aerogel properties. Planet. Space Sci. 57, 58–70. https://doi.org/10.1016/j.pss.2008.11.004.

Burchell, M.J., Fairey, S.A.J., Wozniakiewicz, P., Brownlee, D.E., Hörz, F., Kearsley, A.T., See, T.H., Tsou, P., Westphal, A., Green, S.F., Trigo-Rodríguez, J.M., Domingúez, G., 2008. Characteristics of cometary dust tracks in Stardust aerogel and laboratory calibrations. Meteoritics Planet. Sci. 43, 23–40. https://doi.org/10.1111/j.1945-5100.2008.tb00608.x.

Burchell, M.J., Foster, N.J., Ormond-Prout, J., Dupin, D., Armes, S.P., 2009b. Extent of thermal ablation suffered by model organic microparticles during aerogel capture at hypervelocities. Meteoritics Planet. Sci. 44, 1407–1419. https://doi.org/10.1111/j.1945-5100.2009.tb01182.x.

Burchell, M.J., Graham, G., Kearsley, A., 2006. Cosmic dust collection in aerogel. Annu. Rev. Earth Planet. Sci. 34, 385–418. https://doi.org/10.1146/annurev.earth.34.031405.124939.

Burchell, M.J., Kearsley, A.T., 2009. Short-period Jupiter family comets after Stardust. Planet. Space Sci. 57, 1146–1161. https://doi.org/10.1016/j.pss.2008.07.019.

Campins, H., Hargrove, K., Pinilla-Alonso, N., Howell, E.S., Kelley, M. S., Licandro, J., Mothé-Diniz, T., Fernández, Y., Ziffer, J., 2010. Water ice and organics on the surface of the asteroid 24 Themis. Nature 464, 1320–1321. https://doi.org/10.1038/nature09029.

Christensen, P.R., Jakosky, B.M., Kieffer, H.H., Malin, M.C., McSween Jr., H.Y., Nealson, K., Mehall, G.L., Silverman, S.H., Ferry, S., Caplinger, M., Ravine, M., 2004. The Thermal Emission Imaging System (THEMIS) for the Mars 2001 Odyssey Mission. Space Sci. Rev. 110, 85–130. https://doi.org/10.1023/B:SPAC.0000021008.16305.94.

Cohen, B.A., Coker, R.F., 2000. Modeling of liquid water on CM meteorite parent bodies and implications for amino acid racemization. Icarus 145, 369–381. https://doi.org/10.1006/icar.1999.6329. Available from: <arXiv:physics/9911032>.

Combe, J.P., McCord, T.B., Tosi, F., Ammannito, E., Carrozzo, F.G., De Sanctis, M.C., Raponi, A., Byrne, S., Landis, M.E., Hughson, K.H.G., Raymond, C.A., Russell, C.T., 2016. Detection of local H_2O exposed at the surface of Ceres. Science 353, aaf3010. https://doi.org/10.1126/science.aaf3010.

Donaldson Hanna, K. L., Cheek, L. C., Pieters, C. M., Mustard, J. F., Greenhagen, B. T., Thomas, I. R., Bowles, N.E, 2014. Global assessment of pure crystalline plagioclase across the moon and implications for the evolution of the primary crust. J. Geophys. Res.: Planets 119, 1516–1545.

Drake, M.J., 2005. The Leonard medal address: origin of water in the terrestrial planets. Meteoritics Planet. Sci. 40, 519. https://doi.org/10.1111/j.1945-5100.2005.tb00960.x.

Eberhardt, P., Reber, M., Krankowsky, D., Hodges, R.R., 1995. The D/H and $^{18}O/^{16}O$ ratios in water from comet P/Halley. Astron. Astroph. 302, 301.

Elsila, J.E., Glavin, D.P., Dworkin, J.P., 2009. Cometary glycine detected in samples returned by Stardust. Meteoritics Planet. Sci. 44, 1323–1330. https://doi.org/10.1111/j.1945-5100.2009.tb01224.x.

Emery, J.P., Cruikshank, D.P., Van Cleve, J., 2006. Thermal emission spectroscopy (5.238 μm) of three trojan asteroids with the Spitzer space telescope: Detection of fine-grained silicates. Icarus. 182, 496–512.

Finson, M.J., Probstein, R.F., 1968. A theory of dust comets. I. Model and equations. Astrophys. J. 154, 327–352. https://doi.org/10.1086/149761.

Fujiwara, A., Kawaguchi, J., Yeomans, D.K., Abe, M., Mukai, T., Okada, T., Saito, J., Yano, H., Yoshikawa, M., Scheeres, D.J., Barnouin-Jha, O., Cheng, A.F., Demura, H., Gaskell, R.W., Hirata, N., Ikeda, H., Kominato, T., Miyamoto, H., Nakamura, A.M., Nakamura, R., Sasaki, S., Uesugi, K., 2006. The rubble-pile asteroid Itokawa as observed by Hayabusa. Science 312, 1330–1334. https://doi.org/10.1126/science.1125841.

Genda, H., Ikoma, M., 2008. Origin of the ocean on the Earth: early evolution of water D/H in a hydrogen-rich atmosphere. Icarus 194, 42–52. https://doi.org/10.1016/j.icarus.2007.09.007. Available from: <arXiv:0709.2025>.

Gradie, J., Tedesco, E., 1982. Compositional structure of the asteroid belt. Science 216, 1405–1407. https://doi.org/10.1126/science.216.4553.1405.

Greenhagen, B.T., Lucey, P.G., Wyatt, M.B., Glotch, T.D., Allen, C.C., Arnold, J.A., Bandfield, J.L., Bowles, N.E., Hanna, K.L.D., Hayne, P. O., Song, E., Thomas, I.R., Paige, D.A., 2010. Global silicate mineralogy of the moon from the Diviner lunar radiometer. Science 329, 1507. https://doi.org/10.1126/science.1192196.

Grimm, R.E., McSween Jr., Jr., 1989. Water and the thermal evolution of carbonaceous chondrite parent bodies. Icarus 82, 244–280. https://doi.org/10.1016/0019-1035(89)90038-9.

Hartogh, P., Lis, D.C., Bockelée-Morvan, D., de Val-Borro, M., Biver, N., Küppers, M., Emprechtinger, M., Bergin, E.A., Crovisier, J., Rengel, M., Moreno, R., Szutowicz, S., Blake, G.A., 2011. Ocean-like water in the Jupiter-family comet 103P/Hartley 2. Nature 478, 218–220. https://doi.org/10.1038/nature10519.

Hiroi, T., Zolensky, M.E., Pieters, C.M., Lipschutz, M.E., 1996. Thermal metamorphism of the C, G, B, and F asteroids seen from the 0.7 micron, 3 micron and UV absorption strengths in comparison with carbonaceous chondrites. Meteoritics Planet. Sci. 31, 321–327. https://doi.org/10.1111/j.1945-5100.1996.tb02068.x.

Horner, J., Mousis, O., Hersant, F., 2007. Constraints on the formation regions of comets from their D:H ratios. Earth Moon Planets 100, 43–56. https://doi.org/10.1007/s11038-006-9096-4.

Hörz, F., Bastien, R., Borg, J., Bradley, J.P., Bridges, J.C., Brownlee, D. E., Burchell, M.J., Chi, M., Cintala, M.J., Dai, Z.R., Djouadi, Z., Dominguez, G., Economou, T.E., Fairey, S.A.J., Floss, C., Franchi, I. A., Graham, G.A., Green, S.F., Heck, P., Hoppe, P., Huth, J., Ishii, H., Kearsley, A.T., Kissel, J., Leitner, J., Leroux, H., Marhas, K., Messenger, K., Schwandt, C.S., See, T.H., Snead, C., Stadermann, F. J., Stephan, T., Stroud, R., Teslich, N., Trigo-Rodríguez, J.M., Tuzzolino, A.J., Troadec, D., Tsou, P., Warren, J., Westphal, A., Wozniakiewicz, P., Wright, I., Zinner, E., 2006. Impact Features on Stardust: Implications for Comet 81P/Wild 2 Dust. Science 314, 1716. https://doi.org/10.1126/science.1135705.

Hsieh, H.H., Denneau, L., Wainscoat, R.J., Schörghofer, N., Bolin, B., Fitzsimmons, A., Jedicke, R., Kleyna, J., Micheli, M., Vereš, P., Kaiser, N., Chambers, K.C., Burgett, W.S., Flewelling, H., Hodapp, K.W., Magnier, E.A., Morgan, J.S., Price, P.A., Tonry, J.L., Waters, C., 2015. The main-belt comets: the Pan-STARRS1 perspective. Icarus 248, 289–312. https://doi.org/10.1016/j.icarus.2014.10.031. Available from: <arXiv:1410.5084>.

Hsieh, H.H., Jewitt, D., Ishiguro, M., 2009. Physical properties of main-belt comet P/2005 U1 (Read). Astron. J. 137, 157–168. https://doi.org/10.1088/0004-6256/137/1/157. Available from: <arXiv:0810.1351>.

Hsieh, H.H., Jewitt, D., Lacerda, P., Lowry, S.C., Snodgrass, C., 2010. The return of activity in main-belt comet 133P/Elst-Pizarro. Mon. Not. R. Astron. Soc. 403, 363–377. https://doi.org/10.1111/j.1365-2966.2009.16120.x. Available from: <arXiv:0911.5522>.

Hsieh, H.H., Jewitt, D.C., 2006. A population of comets in the main asteroid belt. Science 312, 561–563.

Hsieh, H.H., Jewitt, D.C., Fernández, Y.R., 2004. The strange case of 133P/Elst-Pizarro: a comet among the asteroids. Astron. J. 127, 2997–3017. https://doi.org/10.1086/383208.

Ikoma, M., Genda, H., 2006. Constraints on the mass of a habitable planet with water of nebular origin. Astrophys. J. 648, 696–706. https://doi.org/10.1086/505780. Available from: <arXiv:astro-ph/0606117>.

Ishii, H.A., Bradley, J.P., 2006. Macroscopic subdivision of silica aerogel collectors for sample return missions. Meteoritics Planet. Sci. 41, 233–236. https://doi.org/10.1111/j.1945-5100.2006.tb00206.x.

Jones, G.H., Knight, M.M., Fitzsimmons, A., Taylor, M.G.G.T., 2017. Cometary science after Rosetta. Philos. Trans. Roy. Soc. London Ser. A 375, 20170001. https://doi.org/10.1098/rsta.2017.0001.

Jones, T.D., Lebofsky, L.A., Lewis, J.S., Marley, M.S., 1990. The composition and origin of the C, P, and D asteroids – water as a tracer of thermal evolution in the outer belt. Icarus 88, 172–192. https://doi.org/10.1016/0019-1035(90)90184-B.

Kaasalainen, M., Torppa, J., 2001. Optimization methods for asteroid lightcurve inversion. I. Shape determination. Icarus 153, 24–36. https://doi.org/10.1006/icar.2001.6673.

Kearsley, A.T., Burchell, M.J., Hörz, F., Cole, M.J., Schwandt, C.S., 2006. Laboratory simulation of impacts on aluminum foils of the Stardust spacecraft: calibration of dust particle size from comet Wild-2. Meteoritics Planet. Sci. 41, 167–180. https://doi.org/10.1111/j.1945-5100.2006.tb00201.x.

Kearsley, A.T., Burchell, M.J., Price, M.C., Graham, G.A., Wozniakiewicz, P.J., Cole, M.J., Foster, N.J., Teslich, N., 2009. Interpretation of Wild 2 dust fine structure: comparison of Stardust aluminum foil craters to the three-dimensional shape of experimental impacts by artificial aggregate particles and meteorite powders. Meteoritics Planet. Sci. 44, 1489–1509. https://doi.org/10.1111/j.1945-5100.2009.tb01188.x.

Kearsley, A.T., Graham, G.A., Burchell, M.J., Cole, M.J., Dai, Z.R., Teslich, N., Bradley, J.P., Chater, R., Wozniakiewicz, P.A., Spratt, J., Jones, G., 2007. Analytical scanning and transmission electron microscopy of laboratory impacts on Stardust aluminum foils: interpreting impact crater morphology and the composition of impact residues. Meteoritics Planet. Sci. 42, 191–210. https://doi.org/10.1111/j.1945-5100.2007.tb00227.x. Available from: <arXiv:astro-ph/0612013>.

Keller, H.U., Arpigny, C., Barbieri, C., Bonnet, R.M., Cazes, S., Coradini, M., Cosmovici, C.B., Delamere, W.A., Huebner, W.F., Hughes, D.W., Jamar, C., Malaise, D., Reitsema, H.J., Schmidt, H.U., Schmidt, W.K.H., Seige, P., Whipple, F.L., Wilhelm, K., 1986. First Halley multicolour camera imaging results from Giotto. Nature 321, 320–326. https://doi.org/10.1038/321320a0.

Keller, L.P., Bajt, S., Baratta, G.A., Borg, J., Bradley, J.P., Brownlee, D. E., Busemann, H., Brucato, J.R., Burchell, M., Colangeli, L., D'Hendecourt, L., Djouadi, Z., Ferrini, G., Flynn, G., Franchi, I.A., Fries, M., Grady, M.M., Graham, G.A., Grossemy, F., Kearsley, A., Matrajt, G., Nakamura-Messenger, K., Mennella, V., Nittler, L., Palumbo, M.E., Stadermann, F.J., Tsou, P., Rotundi, A., Sandford, S. A., Snead, C., Steele, A., Wooden, D., Zolensky, M., 2006. Infrared spectroscopy of Comet 81P/Wild 2 samples returned by Stardust. Science 314, 1728. https://doi.org/10.1126/science.1135796.

Kistler, S.S., 1931. Coherent expanded aerogels and jellies. Nature 127, 741. https://doi.org/10.1038/127741a0.

Kruijer, T.S., Burkhardt, C., Budde, G., Kleine, T., 2017. Age of Jupiter inferred from the distinct genetics and formation times of meteorites. Proc. Natl. Acad. Sci. 114, 6712–6716. https://doi.org/10.1073/pnas.1704461114.

Küppers, M., O'Rourke, L., Bockelée-Morvan, D., Zakharov, V., Lee, S., von Allmen, P., Carry, B., Teyssier, D., Marston, A., Müller, T., Crovisier, J., Barucci, M.A., Moreno, R., 2014. Localized sources of water vapour on the dwarf planet (1)Ceres. Nature 505, 525–527. https://doi.org/10.1038/nature12918.

Lebofsky, L.A., 1980. Infrared reflectance spectra of asteroids – a search for water of hydration. Astron. J. 85, 573–585. https://doi.org/10.1086/112714.

Lebofsky, L.A., Feierberg, M.A., Tokunaga, A.T., Larson, H.P., Johnson, J.R., 1981. The 1.7- to 4.2-micron spectrum of asteroid 1 Ceres - Evidence for structural water in clay minerals. Icarus 48, 453–459. doi: https://doi.org/10.1016/0019-1035(81)90055-5.

Li, J.Y., A'Hearn, M.F., Belton, M.J.S., Farnham, T.L., Klaasen, K.P., Sunshine, J.M., Thomas, P.C., Veverka, J., 2013. Photometry of the nucleus of Comet 9P/Tempel 1 from Stardust-NExT flyby and the implications. Icarus 222, 467–476. https://doi.org/10.1016/j.icarus.2012.02.011.

Lis, D.C., Biver, N., Bockelée-Morvan, D., Hartogh, P., Bergin, E.A., Blake, G.A., Crovisier, J., de Val-Borro, M., Jehin, E., Küppers, M., Manfroid, J., Moreno, R., Rengel, M., Szutowicz, S., 2013. A herschel study of D/H in water in the Jupiter-family Comet 45P/Honda-Mrkos-Pajdušáková and prospects for D/H measurements with CCAT. ApJL 774, L3. https://doi.org/10.1088/2041-8205/774/1/L3. Available from: <arXiv:1307.6869>.

Marty, B., Altwegg, K., Balsiger, H., Bar-Nun, A., Bekaert, D.V., Berthelier, J.J., Bieler, A., Briois, C., Calmonte, U., Combi, M., De Keyser, J., Fiethe, B., Fuselier, S.A., Gasc, S., Gombosi, T.I., Hansen, K.C., Hässig, M., Jäckel, A., Kopp, E., Korth, A., Le Roy, L., Mall, U., Mousis, O., Owen, T., Rème, H., Rubin, M., Sémon, T., Tzou, C. Y., Waite, J.H., Wurz, P., 2017. Xenon isotopes in 67P/Churyumov-Gerasimenko show that comets contributed to Earth's atmosphere. Science 356, 1069–1072. https://doi.org/10.1126/science.aal3496.

Marty, B., Avice, G., Sano, Y., Altwegg, K., Balsiger, H., Hässig, M., Morbidelli, A., Mousis, O., Rubin, M., 2016. Origins of volatile elements (H, C, N, noble gases) on Earth and Mars in light of recent

results from the ROSETTA cometary mission. Earth Planet. Sci. Lett. 441, 91–102. https://doi.org/10.1016/j.epsl.2016.02.031.

McDonnell, J.A.M., Evans, G.C., Evans, S.T., Alexander, W.M., Burton, W.M., Firth, J.G., Bussoletti, E., Grard, R.J.L., Hanner, M.S., Sekanina, Z., 1987. The dust distribution within the inner coma of comet P/Halley 1982i - Encounter by Giotto's impact detectors. Astron. Astroph. 187, 719–741.

McKeegan, K., Aléon, J., Bradley, J., Brownlee, D., Busemann, H., Butterworth, A., Chaussidon, M., Fallon, S., Floss, C., Gilmour, J., Gounelle, M., Graham, G., Guan, Y., Heck, P.R., Hoppe, P., Hutcheon, I.D., Huth, J., Ishii, H., Ito, M., Jacobsen, S., Kearsley, A., Leshin, L.A., Liu, M.C., Lyon, a., Marhas, K., Marty, B., Matrajt, G., Meibom, A., Messenger, S., Mostefaoui, S., Mukhopadhyay, S., Nakamura-Messenger, K., Nittler, L., Palma, R., Pepin, R.O., Papanastassiou, D.A., Robert, F., Schlutter, D., Snead, C.J., Stadermann, F., Stroud, R., Tsou, P., Westphal, A., Young, E.D., Ziegler, K., Zimmermann, L., Zinner, E., 2006. Isotopic compositions of cometary matter returned by Stardust. Science 314, 1724. https://doi.org/10.1126/science.1135992.

Meier, R., Owen, T.C., Matthews, H.E., Jewitt, D.C., Bockelee-Morvan, D., Biver, N., Crovisier, J., Gautier, D., 1998. A determination of the HDO/H_2O Ratio in Comet C/1995 O1 (Hale-Bopp). Science 279, 842. https://doi.org/10.1126/science.279.5352.842.

Morbidelli, A., Bitsch, B., Crida, A., Gounelle, M., Guillot, T., Jacobson, S., Johansen, A., Lambrechts, M., Lega, E., 2016. Fossilized condensation lines in the solar system protoplanetary disk. Icarus 267, 368–376. https://doi.org/10.1016/j.icarus.2015.11.027. Available from: <arXiv:1511.06556>.

Morbidelli, A., Chambers, J., Lunine, J.I., Petit, J.M., Robert, F., Valsecchi, G.B., Cyr, K.E., 2000. Source regions and time scales for the delivery of water to Earth. Meteoritics Planet. Sci. 35, 1309–1320. https://doi.org/10.1111/j.1945-5100.2000.tb01518.x.

Mousis, O., Alibert, Y., 2005. On the composition of ices incorporated in Ceres. Mon. Not. R. Astron. Soc. 358, 188–192. https://doi.org/10.1111/j.1365-2966.2005.08777.x. Available from: <arXiv:astro-ph/0501118>.

Mousis, O., Gautier, D., Bockelée-Morvan, D., Robert, F., Dubrulle, B., Drouart, A., 2000. Constraints on the formation of Comets from D/H ratios measured in H_2O and HCN. Icarus 148, 513–525. https://doi.org/10.1006/icar.2000.6499.

Müller, I., 1999. Speeds of propagation in classical and relativistic extended thermodynamics. Living Rev. Relativ. 2, 1. https://doi.org/10.12942/lrr-1999-1.

Muralidharan, K., Deymier, P., Stimpfl, M., de Leeuw, N.H., Drake, M. J., 2008. Origin of water in the inner solar system: a kinetic monte carlo study of water adsorption on forsterite. Icarus 198, 400–407. https://doi.org/10.1016/j.icarus.2008.07.017.

Nathues, A., Hoffmann, M., Schaefer, M., Le Corre, L., Reddy, V., Platz, T., Cloutis, E.A., Christensen, U., Kneissl, T., Li, J.Y., Mengel, K., Schmedemann, N., Schaefer, T., Russell, C.T., Applin, D.M., Buczkowski, D.L., Izawa, M.R.M., Keller, H.U., O'Brien, D.P., Pieters, C.M., Raymond, C.A., Ripken, J., Schenk, P.M., Schmidt, B. E., Sierks, H., Sykes, M.V., Thangjam, G.S., Vincent, J.B., 2015. Sublimation in bright spots on (1) Ceres. Nature 528, 237–240. https://doi.org/10.1038/nature15754.

O'Brien, D.P., Morbidelli, A., Levison, H.F., 2006. Terrestrial planet formation with strong dynamical friction. Icarus 184, 39–58. https://doi.org/10.1016/j.icarus.2006.04.005.

O'Brien, D.P., Walsh, K.J., Morbidelli, A., Raymond, S.N., Mandell, A. M., 2014. Water delivery and giant impacts in the Grand Tack scenario. Icarus 239, 74–84. https://doi.org/10.1016/j.icarus.2014.05.009.

Ogliore, R.C., Butterworth, A.L., Fakra, S.C., Gainsforth, Z., Marcus, M. A., Westphal, A.J., 2010. Comparison of the oxidation state of Fe in comet 81P/Wild 2 and chondritic-porous interplanetary dust particles. Earth Planet. Sci. Lett. 296, 278–286. https://doi.org/10.1016/j.epsl.2010.05.011. Available from: <arXiv:1005.3858>.

Oka, A., Nakamoto, T., Ida, S., 2011. Evolution of snow line in optically thick protoplanetary disks: effects of water ice opacity and dust grain size. Astrophys. J. 738, 141. https://doi.org/10.1088/0004-637X/738/2/141. Available from: <arXiv:1106.2682>.

Paige, D.A., Siegler, M.A., Zhang, J.A., Hayne, P.O., Foote, E.J., Bennett, K.A., Vasavada, A.R., Greenhagen, B.T., Schofield, J.T., McCleese, D.J., Foote, M.C., DeJong, E., Bills, B.G., Hartford, W., Murray, B.C., Allen, C.C., Snook, K., Soderblom, L.A., Calcutt, S., Taylor, F.W., Bowles, N.E., Bandfield, J.L., Elphic, R., Ghent, R., Glotch, T.D., Wyatt, M.B., Lucey, P.G., 2010. Diviner lunar radiometer observations of cold traps in the moon's south polar region. Science 330, 479. https://doi.org/10.1126/science.1187726.

Platz, T., Nathues, A., Schorghofer, N., Preusker, F., Mazarico, E., Schröder, S.E., Byrne, S., Kneissl, T., Schmedemann, N., Combe, J.P., Schäfer, M., Thangjam, G.S., Hoffmann, M., Gutierrez-Marques, P., Landis, M.E., Dietrich, W., Ripken, J., Matz, K.D., Russell, C.T., 2016. Surface water-ice deposits in the northern shadowed regions of Ceres. Nat. Astron. 1, 0007. https://doi.org/10.1038/s41550-016-0007.

Raymond, S.N., Izidoro, A., 2017. Origin of water in the inner solar system: planetesimals scattered inward during Jupiter and Saturn's rapid gas accretion. Icarus 297, 134–148. https://doi.org/10.1016/j.icarus.2017.06.030. Available from: <arXiv:1707.01234>.

Raymond, S.N., Quinn, T., Lunine, J.I., 2004. Making other Earths: dynamical simulations of terrestrial planet formation and water delivery. Icarus 168, 1–17. https://doi.org/10.1016/j.icarus.2003.11.019. Available from: <arXiv:astro-ph/0308159>.

Rivkin, A.S., Emery, J.P., 2010. Detection of ice and organics on an asteroidal surface. Nature 464, 1322–1323. https://doi.org/10.1038/nature09028.

Robert, F., 2001. Isotope geochemistry: the origin of water on Earth. Science 293, 1056–1058. https://doi.org/10.1126/science.1064051.

Robert, F., Gautier, D., Dubrulle, B., 2000. The solar system D/H ratio: observations and theories. Space Sci. Rev. 92, 201–224. https://doi.org/10.1023/A:1005291127595.

Sandford, S.A., Aléon, J., Alexander, C.M.O., Araki, T., Bajt, S., Baratta, G.A., Borg, J., Bradley, J.P., Brownlee, D.E., Brucato, J.R., Burchell, M.J., Busemann, H., Butterworth, A., Clemett, S.J., Cody, G., Colangeli, L., Cooper, G., D'Hendecourt, L., Djouadi, Z., Dworkin, J.P., Ferrini, G., Fleckenstein, H., Flynn, G.J., Franchi, I.A., Fries, M., Gilles, M.K., Glavin, D.P., Gounelle, M., Grossemy, F., Jacobsen, C., Keller, L.P., Kilcoyne, A.L.D., Leitner, J., Matrajt, G., Meibom, A., Mennella, V., Mostefaoui, S., Nittler, L.R., Palumbo, M.E., Papanastassiou, D.A., Robert, F., Rotundi, A., Snead, C.J., Spencer, M.K., Stadermann, F.J., Steele, A., Stephan, T., Tsou, P., Tyliszczak, T., Westphal, A.J., Wirick, S., Wopenka, B., Yabuta, H., Zare, R.N., Zolensky, M.E., 2006. Organics Captured from Comet 81P/Wild 2 by the Stardust Spacecraft. Science 314, 1720. doi:https://doi.org/10.1126/science.1135841.

Sasselov, D.D., Lecar, M., 2000. On the snow line in dusty protoplanetary disks. Astrophys. J. 528, 995–998. https://doi.org/10.1086/308209. Available from: <arXiv:astro-ph/9911390>.

Schmitz, S., Brenker, F.E., Schoonjans, T., Vekemans, B., Silversmit, G., Vincze, L., Burghammer, M., Riekel, C., 2009. In situ identification of a CAI candidate in 81P/Wild 2 cometary dust by confocal high resolution synchrotron X-ray fluorescence. Geochim. Cosmochim. Acta 73, 5483–5492. https://doi.org/10.1016/j.gca.2009.06.008.

Schorghofer, N., 2008. The lifetime of ice on main belt asteroids. Astrophys. J. 682, 697–705. https://doi.org/10.1086/588633.

Sierks, H., Barbieri, C., Lamy, P.L., Rodrigo, R., Koschny, D., Rickman, H., Keller, H.U., Agarwal, J., A'Hearn, M.F., Angrilli, F., Auger, A. T., Barucci, M.A., Bertaux, J.L., Bertini, I., Besse, S., Bodewits, D., Capanna, C., Cremonese, G., Da Deppo, V., Davidsson, B., Debei, S., De Cecco, M., Ferri, F., Fornasier, S., Fulle, M., Gaskell, R., Giacomini, L., Groussin, O., Gutierrez-Marques, P., Gutiérrez, P.J., Güttler, C., Hoekzema, N., Hviid, S.F., Ip, W.H., Jorda, L., Knollenberg, J., Kovacs, G., Kramm, J.R., Kührt, E., Küppers, M., La Forgia, F., Lara, L.M., Lazzarin, M., Leyrat, C., Lopez Moreno, J.

J., Magrin, S., Marchi, S., Marzari, F., Massironi, M., Michalik, H., Moissl, R., Mottola, S., Naletto, G., Oklay, N., Pajola, M., Pertile, M., Preusker, F., Sabau, L., Scholten, F., Snodgrass, C., Thomas, N., Tubiana, C., Vincent, J.B., Wenzel, K.P., Zaccariotto, M., Pätzold, M., 2015. On the nucleus structure and activity of comet 67P/Churyumov-Gerasimenko. Science 347, aaa1044. doi:https://doi.org/10.1126/science.aaa1044.

Sierks, H., Keller, H.U., Jaumann, R., Michalik, H., Behnke, T., Bubenhagen, F., Büttner, I., Carsenty, U., Christensen, U., Enge, R., Fiethe, B., Gutiérrez Marqués, P., Hartwig, H., Krüger, H., Kühne, W., Maue, T., Mottola, S., Nathues, A., Reiche, K.U., Richards, M. L., Roatsch, T., Schröder, S.E., Szemerey, I., Tschentscher, M., 2011. The Dawn framing camera. Space Sci. Rev. 163, 263–327. https://doi.org/10.1007/s11214-011-9745-4.

Sierks, H., Lamy, P., Barbieri, C., Koschny, D., Rickman, H., Rodrigo, R., A'Hearn, M.F., Angrilli, F., Barucci, M.A., Bertaux, J.L., Bertini, I., Besse, S., Carry, B., Cremonese, G., Da Deppo, V., Davidsson, B., Debei, S., De Cecco, M., De Leon, J., Ferri, F., Fornasier, S., Fulle, M., Hviid, S.F., Gaskell, R.W., Groussin, O., Gutierrez, P., Ip, W., Jorda, L., Kaasalainen, M., Keller, H.U., Knollenberg, J., Kramm, R., Kuhrt, E., Kuppers, M., Lara, L., Lazzarin, M., Leyrat, C., Moreno, J. J.L., Magrin, S., Marchi, S., Marzari, F., Massironi, M., Michalik, H., Moissl, R., Naletto, G., Preusker, F., Sabau, L., Sabolo, W., Scholten, F., Snodgrass, C., Thomas, N., Tubiana, C., Vernazza, P., Vincent, J. B., Wenzel, K.P., Andert, T., Patzold, M., Weiss, B.P., 2011. Images of asteroid 21 Lutetia: a remnant planetesimal from the early solar system. Science 334, 487–490. https://doi.org/10.1126/science.1207325.

Snodgrass, C., Agarwal, J., Combi, M., Fitzsimmons, A., Guilbert-Lepoutre, A., Hsieh, H.H., Hui, M.T., Jehin, E., Kelley, M.S.P., Knight, M.M., Opitom, C., Orosei, R., de Val-Borro, M., Yang, B., 2017. The main belt comets and ice in the solar system. A&A Rev. 25, 5. https://doi.org/10.1007/s00159-017-0104-7. Available from: <arXiv:1709.05549>.

Snodgrass, C., Jones, G., Boehnhardt, H., Gibbings, A., Homeister, M., et al., 2018. The Castalia mission to main belt comet 133p/Elst-Pizarro. Adv. Space Res. 62, 1947–1976. https://doi.org/10.1016/j.asr.2017.09.011.

Soderblom, L.A., Becker, T.L., Bennett, G., Boice, D.C., Britt, D.T., Brown, R.H., Buratti, B.J., Isbell, C., Giese, B., Hare, T., Hicks, M.D., Howington-Kraus, E., Kirk, R.L., Lee, M., Nelson, R.M., Oberst, J., Owen, T.C., Rayman, M.D., Sandel, B.R., Stern, S.A., Thomas, N., Yelle, R.V., 2002. Observations of Comet 19P/Borrelly by the miniature integrated camera and spectrometer aboard deep space 1. Science 296, 1087–1091. https://doi.org/10.1126/science.1069527.

Spencer, J.R., Denk, T., 2010. Formation of Iapetus' extreme albedo dichotomy by exogenically triggered thermal ice migration. Science 327, 432. https://doi.org/10.1126/science.1177132.

Spencer, J.R., Lebofsky, L.A., Sykes, M.V., 1989. Systematic biases in radiometric diameter determinations. Icarus 78, 337–354. https://doi.org/10.1016/0019-1035(89)90182-6.

Stimpfl, M., Walker, A.M., Drake, M.J., de Leeuw, N.H., Deymier, P., 2006. An ångström-sized window on the origin of water in the inner solar system: atomistic simulation of adsorption of water on olivine. J. Cryst. Growth 294, 83–95. https://doi.org/10.1016/j.jcrysgro.2006.05.057.

Taylor, M.G.G.T., Altobelli, N., Buratti, B.J., Choukroun, M., 2017. The Rosetta mission orbiter Science overview the comet phase. Phil. Trans. Royal Soc. A 375, 20160262. https://doi.org/10.1098/rsta.2016.0262.

Thomas, I.R., Bowles, N.E., Greenhagen, B.T., Glotch, T.D., Donaldson Hanna, K.L., Wyatt, M.B., Bandfield, J.L., Paige, D.A., 2010. Emission measurements of lunar analogues for interpretation of returning data from the diviner lunar radiometer on NASA's lunar reconnaissance orbiter. In: Lunar and Planetary Science Conference, p. 1364.

Thomas, N., Barbieri, C., Keller, H., Lamy, P., Rickman, H., Rodrigo, R., Sierks, H., Wenzel, K., Cremonese, G., Jorda, L., Küppers, M., Marchi, S., Marzari, F., Massironi, M., Preusker, F., Scholten, F., Stephan, K., Barucci, M., Besse, S., El-Maarry, M., Fornasier, S., Groussin, O., Hviid, S., Koschny, D., Kührt, E., Martellato, E., Moissl, R., Snodgrass, C., Tubiana, C., Vincent, J.B., 2012. The geomorphology of (21) Lutetia: Results from the OSIRIS imaging system onboard ESA's Rosetta spacecraft. Planet. Space Sci. 66, 96–124. https://doi.org/10.1016/j.pss.2011.10.003.

Thomas, P.C., Parker, J.W., McFadden, L.A., Russell, C.T., Stern, S.A., Sykes, M.V., Young, E.F., 2005. Differentiation of the asteroid Ceres as revealed by its shape. Nature 437, 224–226. https://doi.org/10.1038/nature03938.

Trigo-Rodríguez, J.M., Domínguez, G., Burchell, M.J., Hörz, F., Llorca, J., 2008. Bulbous tracks arising from hypervelocity capture in aerogel. Meteoritics Planet. Sci. 43, 75–86. https://doi.org/10.1111/j.1945-5100.2008.tb00610.x.

Tsou, P., Brownlee, D.E., Sandford, S.A., Hörz, F., Zolensky, M.E., 2003. Wild 2 and interstellar sample collection and Earth return. J. Geophys. Res. (Planets) 108, 8113. https://doi.org/10.1029/2003JE002109.

Vernazza, P., Fulvio, D., Brunetto, R., Emery, J.P., Dukes, C.A., Cipriani, F., Witasse, O., Schaible, M.J., Zanda, B., Strazzulla, G., Baragiola, R.A., 2013. Paucity of Tagish lake-like parent bodies in the asteroid belt and among Jupiter Trojans. Icarus 225, 517–525. https://doi.org/10.1016/j.icarus.2013.04.019.

Vilas, F., Jarvis, K.S., Gaffey, M.J., 1994. Iron alteration minerals in the visible and near-infrared spectra of low-albedo asteroids. Icarus 109, 274–283. https://doi.org/10.1006/icar.1994.1093.

Villanueva, G.L., Mumma, M.J., Bonev, B.P., Di Santi, M.A., Gibb, E.L., Böhnhardt, H., Lippi, M., 2009. A sensitive search for deuterated water in Comet 8P/Tuttle. Astrophys. J. Lett. 690, L5–L9. https://doi.org/10.1088/0004-637X/690/1/L5.

Walsh, K.J., Morbidelli, A., Raymond, S.N., O'Brien, D.P., Mandell, A. M., 2011. A low mass for Mars from Jupiter's early gas-driven migration. Nature 475, 206–209. https://doi.org/10.1038/nature10201. Available from: <arXiv:1201.5177>.

Weaver, H.A., Lisse, C.M., Mutchler, M., Lamy, P.L., Toth, I., Reach, W. T., Vaubaillon, J., 2008. Hubble investigation of the B and G fragments of Comet 73P/Schwassmann-Wachmann 3. In: Asteroids, Comets, Meteors 2008, p. 8248.

Westphal, A.J., Snead, C., Butterworth, A., Graham, G.A., Bradley, J.P., Bajt, S., Grant, P.G., Bench, G., Brennan, S., Pianetta, P., 2004. Aerogel keystones: extraction of complete hypervelocity impact events from aerogel collectors. Meteoritics Planet. Sci. 39, 1375–1386. https://doi.org/10.1111/j.1945-5100.2004.tb00952.x. Available from: <arXiv:astro-ph/0312460>.

Zolensky, M.E., Pieters, C., Clark, B., Papike, J.J., 2000. Invited review small is beautiful: the analysis of nanogram-sized astromaterials. Meteoritics Planet. Sci. 35, 9–29. https://doi.org/10.1111/j.1945-5100.2000.tb01970.x.

Zolensky, M.E., Zega, T.J., Yano, H., Wirick, S., Westphal, A.J., Weisberg, M.K., Weber, I., Warren, J.L., Velbel, M.A., Tsuchiyama, A., Tsou, P., Toppani, A., Tomioka, N., Tomeoka, K., Teslich, N., Taheri, M., Susini, J., Stroud, R., Stephan, T., Stadermann, F.J., Snead, C.J., Simon, S.B., Simionovici, A., See, T.H., Robert, F., Rietmeijer, F.J.M., Rao, W., Perronnet, M.C., Papanastassiou, D.A., Okudaira, K., Ohsumi, K., Ohnishi, I., Nakamura-Messenger, K., Nakamura, T., Mostefaoui, S., Mikouchi, T., Meibom, A., Matrajt, G., Marcus, M.A., Leroux, H., Lemelle, L., Le, L., Lanzirotti, A., Langenhorst, F., Krot, A.N., Keller, L.P., Kearsley, A.T., Joswiak, D., Jacob, D., Ishii, H., Harvey, R., Hagiya, K., Grossman, L., Grossman, J.N., Graham, G.A., Gounelle, M., Gillet, P., Genge, M.J., Flynn, G., Ferroir, T., Fallon, S., Ebel, D.S., Dai, Z.R., Cordier, P., Clark, B., Chi, M., Butterworth, A.L., Brownlee, D.E., Bridges, J.C., Brennan, S., Brearley, A., Bradley, J.P., Bleuet, P., Bland, P.A., Bastien, R., 2006. Mineralogy and petrology of Comet 81P/Wild 2 nucleus samples. Science 314, 1735. doi:https://doi.org/10.1126/science.1135842.